MULTIPLE INPUT MULTIPLE OUTPUT CHANNEL MEASUREMENTS AND SYSTEM PERFORMANCE

Michael Mewburn

A THESIS SUBMITTED IN FULFILMENT OF THE REQUIREMENT FOR THE DEGREE OF MASTER OF ENGINEERING

AT

CENTRE FOR TELECOMMUNICATIONS AND MICRO-ELECTRONICS,
VICTORIA UNIVERSITY
MELBOURNE, AUSTRALIA

2010

DECLARATION

"I, Michael Mewburn, declare that the Master by Research thesis entitled "Multiple Input Multiple Output channel measurements and system performance" is no more than 60,000 words in length, exclusive of tables, figures, appendices, references and footnotes. This thesis contains no material that has been submitted previously, in whole or in part, for the award of any other academic degree or diploma. Except where otherwise indicated, this thesis is my own work".

Michael Mewburn _____

CONTENTS

Contents ii

Abstract v

Acknowledgements vii

Mathematical Notation viii

Chapter 1 1

Introduction 1

1.1 Background 1

1.2 Literature review 3

1.3 Contribution of the thesis 5

1.4 Thesis overview 6

Chapter 2 7

Multiple Input Multiple Output Communication 7

2.1 The motivation for MIMO 8

2.1.1 Limitation of SISO capacity 8
2.1.2 Multipath propagation conditions 9
2.1.3 Coherence bandwidth and time dispersion characteristics of multipath channels. 9
2.2 Operating principles of MIMO Communication systems 12
2.3 Cost / benefit considerations 13
2.4 Propagation model 14
2.5 Singular Value Decomposition 14
2.5.1 Sub channel redundancy 16
2.6 MIMO capacity 16
2.7 Normalisation 18
Chapter 3 20
Hardware Development and Operation 20
3.1 Development goals 21
3.2 Hardware description 22
3.2.1 Receiver 24
Omnidirectional receive array 24
Directional receive array 25
3.2.2 Ancillary Receive array hardware 25
Power supply 26
RF switch 26
RF switch controller 27
Low noise amplifiers 28
3.2.3 Transmitter 29
Displacement accuracy 31
3.2.4 Network Analyser 31
3.2.5 Master PC 32
3.2.6 Measurement Software 32
Data storage 34
3.2.7 Antenna development 35
Discone 35
Circular dipole (directional) array 37
Dual polarised patch 38
3.3 Measurement programs 41
3.4 Measurement protocols 42

3.5 Data quality 43
3.5.1 Hardware Calibration 44
Calibration procedure 45
Chapter 4 48
Results and Analysis 48
4.1 Analysis software 48
4.2 Channel stability 52
4.3 Indoor channel frequency response 53
4.3.1 Variation in measured channel gain 55
4.4 Indoor MIMO channel capacity 55
4.4.1 Path Loss and array element directivity 56
Capacity calculated with fixed SNR 57
Capacity calculated with measured SNR 61
4.4.2 Array element polarisation 63
Transmit array 64
Receive array 65
Results 65
Examination of MIMO gain in isolation 65
Examination of MIMO gain and channel gain combined 66
4.4.3 Channel correlation 66
4.5 Singular value comparison of a range of indoor MIMO channels 68
4.6 Keyhole effect 70
Chapter 5 71
Conclusion 71
Further work 73
Publications 74
References 75
Appendix A 79
Appendix B 84
Appendix C 89
Appendix D 90
Appendix E 91

ABSTRACT

Existing wireless links using a single antenna element at the transmitter and receiver are heavily influenced by the multipath scattering arising from objects in the transmission environment. Unlike conventional systems, a concept referred to as Multiple-Input Multiple-Output or MIMO not only thrives under multipath conditions but also has the potential to allow for substantial increases in capacity. MIMO systems use a combination of multiple antenna arrays at the transmitter and receiver in conjunction with dedicated Digital Signal Processing (DSP). Before MIMO systems are designed and deployed, a database of typical propagation measurements is required to confirm theoretical predictions with reality.

The design, development and use of specialised measurement equipment to accurately establish an indoor MIMO measurement database is presented in this thesis. An extension of this work is the consideration of practical hardware choices (for example antenna type) in an end user implementation.

INFORMATION THEORETIC CAPACITY (MAXIMUM ERROR FREE CAPACITY UTILISING IDEAL CODING) AND SINGULAR VALUE DECOMPOSITION ANALYSIS

ARE THE PRIMARY TOOLS WITH WHICH COMPARISONS BETWEEN THE MEASURED CHANNELS ARE MADE. THIS THESIS DEMONSTRATES THAT FOR THE GIVEN INDOOR PROPAGATION ENVIRONMENT, SIGNAL TO NOISE RATIO IS A SIGNIFICANT DETERMINANT OF INDOOR MIMO CAPACITY AND THAT OMNIDIRECTIONAL ARRAY ELEMENTS AFFORD GREATER MIMO

CAPACITY THAN DIRECTIONAL ALTERNATIVES.ACKNOWL EDGEMENTS

I am indebted to the Australian Telecommunications Cooperative Research Centre for funding assistance with this project and the following people for their generous assistance and support:

My supervisory team of Mike Faulkner, Phil Conder, Terence Betlehem and Ying Tan have gone above and beyond to help ensure the success of this research project and I thank them sincerely

Thanks are also due to the technical support team of Nghia Truong and Donald Ermel. Nghia was most helpful in producing printed circuit boards and running the measurement system, while Donald made his excellent machining skills available in the construction of the antenna positioning system and discone antennas.

Stewart Jenvey from the Centre for Telecommunications and Information Engineering at Monash University generously provided the directional receive array and the services of his anechoic chamber for antenna testing.

Inger Mewburn kindly proofread this work, offering valuable feedback.

Most importantly, I offer my thanks and love to my beautiful wife and friend, Aurora for her understanding and support over the duration of this project.

MATHEMATICAL NOTATION

$\boldsymbol{\alpha}$	n_R x 1 frequency response vector of the low noise amplifiers
$\boldsymbol{\chi}$	aggregate measurement hardware response matrix
g	is the transmit power amplifier response vector
h_{ij}	random fading between the *i*th receive element and the *j*th transmit element
$\mathbf{H}^{\Diamond}$	measured n_R x n_T complex channel matrix - includes hardware artefacts
H	actual channel response matrix - In this work, $\mathbf{H}^{\Diamond}$ after hardware correction
L	n_R x n_R the Insertion loss and leakage matrix of RF switch
i.i.d.	independent and identically distributed
k	number of singular values yielded by SVD(**H**)
n	length n_R AWGN vector
n_R	number of receive antenna elements
n_T	number of transmit antenna elements
ρ	SNR.
s	transmit element separation (number of multiples of λ/4 @ 2.45 GHz)
σ_k	k^{th} singular value
$\boldsymbol{\Sigma}$	diagonal singular value matrix
U	unitary matrix
V	unitary matrix
y	length n_R receive vector
x	length n_T transmit vector

Note to the reader: Sequential numbering of equations is across thesis, not chapter.

Chapter 1

INTRODUCTION

PREFACE

Chapter 1 discusses limitations of traditional wireless communication techniques and proposes an alternative method to improve reliability and data capacity, called multiple input, multiple output, or MIMO. The development and use of MIMO measurement hardware to characterise a typical indoor office propagation environment are presented as the contributions of this research project. The chapter concludes with a thesis overview to acquaint the reader with the document.

1.1 Background

In his classic work of 1948, 'A Mathematical Theory of Communication', [1] Claude Shannon declared "The fundamental problem of communication is that of reproducing at one point either exactly or approximately a message selected at another point." As stated therein, a theoretical maximum capacity (of information transfer in bits/s/Hz) limit exists for a communication system between two points comprising an information source or transmitter, a noisy propagation medium and a receiver,

$$C = BW \log_2(1 + SNR) \quad (1)$$

where the maximum channel capacity, C (bits/s) is proportional to the signal bandwidth, BW (Hz) and received signal to noise ratio, SNR. The wireless system discussed by Shannon consists of a single radiating element at either end of a communication link, now described as single input, single output or SISO.

The escalating consumer demand for reliable, high data rate wireless communication systems has for some time reached and indeed, pushed beyond the boundaries of the Shannon limit. Even with optimal coding and modulation schemes, these SISO communication systems must still comply with Shannon's limit as an upper bound on capacity. The SISO topology has been the benchmark format for telecommunication of the twentieth century but is now being challenged by an alternative scheme, MIMO.

Multiple input, multiple output or MIMO communication systems utilise multiple element antenna arrays at the transmitter and receiver to offer significant capacity gains over SISO. Multiple element arrays have been successfully employed at the receiver for some time in the interests of diversity gain; where the best individual, or an optimal combination of several spatially separated receive elements is selected for maximal SNR. While improved SNR will increase capacity beyond that provided by a true SISO system, the Shannon limit still applies. By contrast, a multiple-input multiple-output (MIMO) system allows the simultaneous parallel transmission of multiple streams of data over the same bandwidth. MIMO has the potential to provide a linear increase in capacity proportional to the smaller number of transmit or receive array elements [2]. Systems employing simple antenna diversity furnish only a logarithmic capacity improvement.

Indoor- and heavily built up outdoor-environments are commonly considered to have *rich* or *dense scattering* properties due to the potentially large number of objects in and around the propagation path. Physical objects may cause reflection, refraction or attenuation (or any combination of the three) in the propagating wave. Attenuation lowers received SNR, in turn reducing capacity for both SISO and MIMO systems. Reflection and refraction can result in multiple time-delayed copies of the transmitted data arriving at the receiver; a phenomenon termed *multipath*. The

arbitrary phase addition at a receive antenna due to multipath results in random fading, or attenuation, of the received signal. Using any of a number of signal processing algorithms, MIMO systems utilise a rich scattering environment to de-correlate signal paths from spatially separated array elements. In addition to the potentially substantial increases in capacity, reliance upon multipath in MIMO inherently provides immunity to it.

A database of typical propagation measurements is required to validate theoretical predictions before the design and deployment of MIMO systems. Early research has depended upon propagation measurements and models based on SISO communication systems, but this lacks important information required for MIMO research. MIMO system designers require intimate knowledge of the propagation channel to evaluate the MIMO capacity improvement over SISO and to determine any hardware and environmental dependency. This project seeks to assess the effects of system characteristics such as antenna type, array configuration [3], access point location and building design and building materials [4] on MIMO systems.

1.2 Literature review

From infancy in the 1970s, the concept of increased capacity using multiple - antenna arrays gained significant momentum from the late 1980s and through the 1990s with seminal works by Winters [5], Foschini & Gans [2] and Telatar [6]. In these papers and numerous others since, channel capacity is examined with the aid of simulated channel responses in the absence of real measurement data.

This project was intended to amend the deficiency of actual measurement results (prior to commencement) available to researchers with an indoor propagation measurement campaign.

Direct MIMO propagation channel measurement [7-12] employing dedicated transmitters and receivers for each array element is the most accurate characterisation technique. Indirect measurement systems use switched (multiplexed) array [13-15], virtual array [13, 15-20] or a combination of both. Indirect systems are realistically restricted to stationary indoor environments due to a susceptibility to temporal variation during measurements, but are typically more cost effective than direct systems to implement.

Literature pertinent to this research usually examines topics such as how synthetic models may be fitted to physical data and how physical parameters such as element spacing and location effect capacity. Much has also been said about the requirement for large amounts of scattering to sufficiently de-correlate the channel [9, 21]. The implication from this is that Non Line of Sight (NLOS) scenarios will be most conducive to MIMO channel capacity as the more highly correlated Line of Sight (LOS) components are not present. Some work has been carried out that suggests this is not always the case [22, 23], where it was found that good signal to noise ratio arising from an LOS scenario can play a significant role in determining capacity.

Some debate also appears evident over the optimum array element spacing [3, 9, 24, 25]. Correlation is shown to increase dramatically with increasing numbers of elements added to the same fixed aperture [24]. Contrary to this, it is claimed in [3] that a capacity increase may be observed between 0.5 and 0.2 wavelengths.

An obvious implication of the use of multiple element arrays in communication systems is the increase in physical array size and hardware complexity as the number of antennas and associated RF chains rises. Multimode MIMO systems have been proposed in [26] and others, where array size is significantly reduced or fully condensed to one element while still retaining the functionality of a full array. This is achieved by exciting two or more electromagnetic modes of the antenna(s); an approach suffering none of the cross coupling inherent between physically separate array elements. The significant benefits of this method are packaging and cost, as the number of transceivers and antenna elements are reduced. Another potential technique for reducing array dimensions is the switched parasitic antenna [27]. Parasitic elements, near the driven element are left open-circuit or shorted, with the number of combinations available corresponding to the number of virtual elements. The primary drawback of this system is the increase in SNR required to achieve the same capacity as a traditional array. Where the principal concern is the number of transceivers and not necessarily array elements, adaptive selection of sub arrays of the main array is made for each of the $x < n_R$ RF chains at the receiver [28].

1.3 Contribution of the thesis

This project is concerned with the development of a MIMO measurement system (and use thereof) to extensively characterise an indoor propagation environment. The principle aims of this research project are:

- Develop a methodology for generating an indoor MIMO measurement database; involving the design, construction and testing of the appropriate radio channel measuring equipment. The accuracy of the measurements should be consistent with current and future requirements of indoor wireless communication systems.
- Undertake several measurement programs to comparatively study the effects of array configuration and array element types for typical indoor conditions.
- Develop Graphical User Interface based software to evaluate the performance of several MIMO systems using the gathered data.

The research project involves the development of a significant amount of hardware for the collection of channel measurements, comprising a mobile transmitter, stationary receiver and network analyser that together, measure the channel gain between each pair of transmit and receive antennas. The receiver is a fixed array where, depending on the array in question, one of four (or one of eight) antenna elements is multiplexed to the network analyser. The transmit array is synthesised with a single antenna mounted on a two-dimensional positioning system.

Purpose-specific software has been written in the MATLAB environment to analyse data measured by the network analyser, allowing comparison between measured channel performance and theoretical predictions of channel capacity. The software calculates and displays time and frequency domain representations, singular value behaviour and channel capacity for the user-defined MIMO channel.

The analysis software, antenna elements, omnidirectional receive array, transmit antenna positioning system and software to control them were developed specifically for this project.

The MIMO measurement database is intended for use by researchers in the development of channel models, the testing of signal processing algorithms, and the deployment of MIMO antenna systems. The measurement data must therefore have

high integrity, requiring careful design and implementation of the channel measurement program. The measurements must be essentially noise free and reproducible.

1.4 Thesis overview

The document is arranged as follows:

Chapter 2 - Multiple Input Multiple Output communication.

The theory and execution of MIMO wireless systems is described. Benefits and limitations of the concept are discussed and relevant literature is reviewed.

Chapter 3 - Hardware development and operation.

The development and implementation of the measurement apparatus is described. Operational requirements of the hardware necessary to achieve the goals of this work are covered. Detailed descriptions are given of individual hardware components and the software written to control them. All the mechanics, electronics, control software and calibration processes were developed by the author.

Chapter 4 - Results and analysis.

The MIMO measurement campaign data is presented and analysed using MATLAB software specially written by the author for the task. Theoretical aspects such as singular value decomposition and the calculation of capacity are discussed. The performance of many indoor MIMO wireless channels is evaluated, primarily in terms of singular value behaviour and MIMO capacity.

Chapter 5 - Conclusions.

Conclusions are drawn and further work proposed

Chapter 2

MULTIPLE INPUT MULTIPLE OUTPUT COMMUNICATION

PREFACE

The previous chapter covered the state of the art at the commencement of this project and discussed the research motivation and direction. Chapter 2 provides insight into the operation of communication systems using MIMO architectures. Some benefits and limitations to the use of multiple antenna arrays are discussed in terms of capacity and propagation environment. Singular value decomposition is presented as a method of analysis of MIMO channels. The chapter is concluded with a discussion of the theoretical maximum MIMO capacity limit.

2.1 The motivation for MIMO

Of particular interest for communication system design is the ability to reliably send and receive data with sufficient capacity (bits/s/Hz). Reliable reception with adequate capacity is of critical importance in typical propagation environments such as office spaces and heavily built up urban areas. The random fading inherent in these conditions reduces the capacity and reliability of reception for traditional SISO communications systems.

2.1.1 Limitation of SISO capacity

The Shannon capacity limit [1] demonstrates direct proportionality between capacity and received SNR. Multipath propagation results in both frequency and spatially selective fading, either of which readily degrades received signal strength. Figure 1 demonstrates that multipath fading could easily account for an SNR deficit of several orders of magnitude.

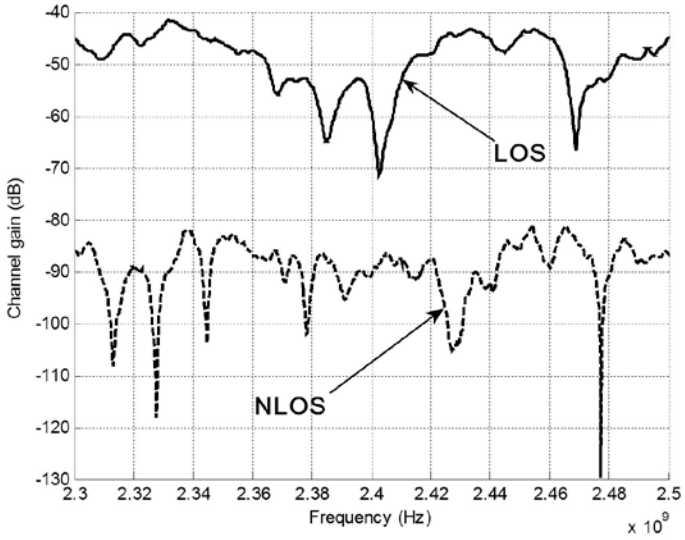

Figure 1: Measured frequency response of a SISO channel for LOS and NLOS environments

For example, (with the exclusion of any coding and modulation gains) a 30 dB fade could reduce SISO capacity by 9.97 bits/s/Hz. The potentially significant constraints on capacity and reliability of SISO systems in multipath propagation environments led to a need for research into the MIMO technique.

2.1.2 Multipath propagation conditions

Unimpeded propagation between transmitter and receiver is termed line of sight (LOS), while physical objects in the propagation path create non line of sight (NLOS) conditions. Figure 1 presents a comparison of measured SISO channels (using the apparatus described in chapter 3) for LOS and NLOS propagation environments.

Measurements were taken with the transmitter in the same room as the receiver for the LOS data and a different room for the NLOS case. The dominant main signal and moderate multipath (in this example due to furniture and other internal surfaces) characteristics of LOS transmission result in a comparatively high average power and lower number of deep fades. The presence of dividing walls and greater displacement between the transmitter and receiver are responsible for the loss of received power and increased incidence and magnitude of fades in the NLOS case.

2.1.3 Coherence bandwidth and time dispersion characteristics of multipath channels.

Received signals experience *flat fading* if the transmitted signal bandwidth is less than the coherence bandwidth (B_c) of the channel [29]; that is, the maximum bandwidth for which gain is constant and phase is linear. In contrast, *frequency selective fading* results from a transmission bandwidth greater than the coherence bandwidth. All frequencies within B_c will exhibit correlated amplitude as they are identically affected by the propagation channel. A pair of sinusoids with spectral separation greater than B_c is likely to exhibit non-correlated amplitude or frequency selective fading. The full measurement bandwidth of 200 MHz depicted in Figure 1 is much greater than B_c for both LOS and NLOS examples, as frequency selective fading is evident for each.

For the case of the correlation function over time of two signals equal to or greater than 0.9, B_c may be approximated by [29]:

$$B_c \approx \frac{1}{50\sigma_t} \tag{2}$$

A normalised power delay profile may be used to determine the rms delay spread, σ_t, commonly used to characterise the temporal behaviour of a wideband multipath propagation channel. Rappaport [29] notes that a power delay profile is derived from an average of impulse response measurements in space or time taken in a given a local area. While Figure 1 demonstrates the frequency response behaviour of two distinct indoor propagation channels between a single transmitter-receiver pair, Figure 2 presents a normalised power delay profile, averaged over 260 channel realisations, for the same LOS and NLOS locations.

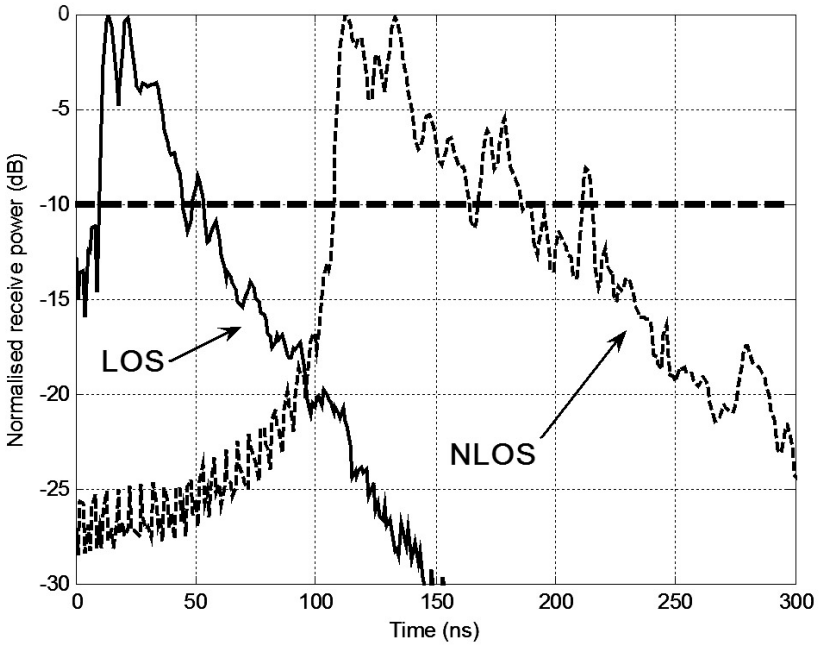

Figure 2: Measured power delay profile (normalised to 0 dB) for line of sight (LOS) and non line of sight (NLOS) propagation environments, showing -10 dB threshold used to calculate time dispersion parameters. Transmit and receive arrays employed omnidirectional elements.

Several features of note are apparent in Figure 2:

- Exponential decay is observed.
- Transmitter to receiver displacement is less in the LOS case.
- The intuitive expectation of greater delay spread arising from increased multipath is evident in the relative time dilation of the NLOS trace.

The rms delay spread, σ_t is defined [29] as the square root of the second central moment of the power delay profile;

$$\sigma_\tau = \sqrt{\overline{\tau^2} - \left(\overline{\tau}\right)^2} \tag{3}$$

The first moment of the power delay profile, or *mean excess delay*, $\overline{\tau}$ is found with

$$\overline{\tau} = \frac{\sum_k P(\tau_k)\tau_k}{\sum_k P(\tau_k)}$$

and the second moment, $\overline{\tau^2}$, by

$$\overline{\tau^2} = \frac{\sum_k P(\tau_k)\tau_k^2}{\sum_k P(\tau_k)}$$

$P(\tau_k)$ refers to a multipath signal arriving τ_k after the first received peak at $\tau_0 = 0$. The total time multipath energy is received above a defined threshold (chosen to differentiate multipath components from thermal noise) is referred to as the *maximum excess delay*.

Time dispersion parameters calculated from Figure 2 for a power threshold of -10 dB are shown in Table 1.

Table 1: Calculated time dispersion parameters relating to Figure 2

INDOOR CHANNEL TYPE	**LOS**	**NLOS**
MAXIMUM EXCESS DELAY (ns)	43	107
MEAN EXCESS DELAY (ns)	14.7	28.7
σ_t **(ns)**	9.9	22.9
$\boldsymbol{B_c}$ **(KHz)**	2020	873

Measured channel data demonstrate degradation in B_c as indoor channels become NLOS, corresponding to an increase in multipath and received delay spread. Based on measurement results published in [29-31] and other sources, a delay spread of 200 ns is proposed as an approximate delineation between indoor and outdoor propagation channels in the upper UHF frequencies, with σ_{indoor} commonly below 50 ns in the references mentioned. The measured results presented in Table 1 are thus in broad agreement with published data.

Field Code Changed

Both measured and published data suggest that traditional SISO communications systems tend to exhibit reduced capacity in the presence of multipath. Conversely, the alternative strategy of MIMO, with a demonstrated immunity to multipath, has generated immense interest.

2.2 Operating principles of MIMO Communication systems

The MIMO method of data transmission evolved to combat the capacity limit and multipath sensitivity inherent in SISO. MIMO employs a combination of hardware and software to generate an increase in channel capacity (bits/s/Hz) over SISO systems and to confer immunity to multipath in rich scattering indoor and outdoor environments. Physically, a multiple element array with transceiver hardware for each element is deployed at both ends of a communication link, with issues such as modulation schemes, channel estimation and power allocation handled in software.

The conventional format to describe the dimension of a MIMO system is n_R x n_T, where n_R is the number of receive and n_T the number of transmit elements. An extension to the standard nomenclature is introduced to clarify systems employing multiple polarisations discussed later in this work. The n_R x n_T format is retained, with the number of polarisations greater than one shown in subscript. For example, 4 x 2_2 describes two dual-polarised transmit elements and four single polarised receive elements.

The most trivial manifestation of MIMO has four individual paths between transmitter and receiver. Figure 3 depicts the entries of a 2 x 2[†] channel response matrix, **H**, where h_{ij} represents the flat fading gain between transmit element *j* to receive element *i*.

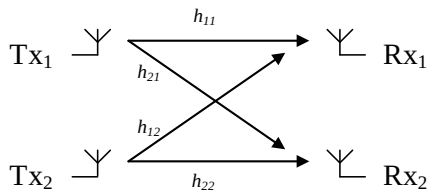

Figure 3: Schematic representation of a 2x2 MIMO channel representation

Uncorrelated entries in the channel response matrix are central to the operation of MIMO, permitting conveyance of separate and independent information sets from multiple transmit elements at the same frequency at the same time. As the entries of **H** become fully decorrelated, MIMO capacity approaches a potential maximum of min (n_R,n_T) x SISO capacity.

To successfully decode incoming MIMO data in an actual system, the receiver must know the effect of the propagation channel on **H**, so a known preamble is sent on each transmit antenna. Incoming data is then decoded with this knowledge for as long as the channel is considered coherent. The receiver decodes the separate streams of information using one of a number of possible signal processing algorithms.

2.3 Cost / benefit considerations

Despite the proposed benefits, the implementation of MIMO systems may be impeded by greater cost, packaging and signal processing issues than for SISO. Generally, the use of an *n* x *n* MIMO system requires *n* separate transceiver chains, *n* element arrays and suitable signal processing hardware and software at each end of the communication link.

In contrast, the significant capacity advantage and multipath immunity of MIMO may reasonably be expected to be of higher importance than the physical

[†] Equivalent systems with multiple polarisations are 1_2 x 1_2, 2 x 1_2 or 1_2 x 2.

packaging and financial costs of implementation in many cases. The preceding discussion has espoused the improvements to reliability of service and capacity for a given user with the adoption of MIMO architecture. MIMO may also be used to improve reliability of service for other users of the same band in the same local area. Transmit power, bandwidth or a combination of both could be reduced in a MIMO system to decrease interference between users, while still achieving or exceeding capacity identical to that of a SISO system.

2.4 Propagation model

Consider a multiple input multiple output communications channel, accessed by n_R receive elements and n_T transmit elements. The channel is assumed to exhibit flat frequency fading, with packets short enough that any communication occurs within the coherence time, T_c of the channel. Equal power allocation is employed across all transmit elements and additive white Gaussian noise (AWGN) is the only additive signal at the receiver, as no more than one user transmits at any on time.

The complex baseband equivalent model of this system is given by [32]:

$$\mathbf{y} = \mathbf{H}\mathbf{x} + \mathbf{n} \tag{4}$$

where **x** is the length n_T transmit vector, **y** is the length n_R receive vector, **H** is the n_R x n_T complex channel matrix where h_{ij} represents the random i.i.d. fading between the i^{th} receive element and the j^{th} transmit element and **n** is a length n_R AWGN vector.

2.5 Singular Value Decomposition

A common method of analysis of MIMO systems is Singular value decomposition (SVD) of the channel matrix. SVD generates $k = \min(n_R, n_T)$ singular values, σ, which represent the voltage gains of the virtual SISO channels between the transmitter and receiver. SVD of **H** yields:

$$\text{SVD}(\mathbf{H}) = \mathbf{U}\mathbf{\Sigma}\mathbf{V}^{\dagger} \tag{5}$$

where **U** and **V** are unitary matrices; n_R x n_R and n_T x n_T in size, respectively. **U** and **V** are known as the left and right singular matrices. $[.]^\dagger$ is the conjugate transpose operator. Each of the *k* descending diagonal entries of **Σ** is an ordered singular value of **H**, where **Σ** has the same dimension and rank as **H**. Matrix rank provides a measure of the maximum number of linearly independent columns or rows. The greatest achievable rank for a given matrix is equal to the smaller number of columns or rows. A matrix of *full rank* has completely independent entries, while a *rank deficient* matrix exhibits some degree of correlation.

With regards to MIMO, increasing decorrelation of the channel encourages full rank n_R x n_T channel matrices. Correspondingly, the number of singular values and thus, sub channels, is maximised to the smaller number of transmit or receive elements with propagation channel decorrelation. The *keyhole* or *pinhole effect* is a notable exception to this generalisation; whereby uncorrelated channel transfer matrices exhibit low rank [18]. Diffraction around corners and waveguiding effects from propagation along hallways or narrow streets is one determinant of keyhole behaviour.

Considering (4) and (5); decomposition of the channel matrix into independent sub-channels is achieved by filtering the transmitted and received signals with **V** and $\mathbf{U}^\dagger$, respectively [32].

$$\mathbf{U}^\dagger\mathbf{y} = \mathbf{U}^\dagger(\mathbf{HVx} + \mathbf{n})$$
$$\mathbf{U}^\dagger\mathbf{y} = \mathbf{U}^\dagger(\mathbf{U\Sigma V}^\dagger\mathbf{Vx} + \mathbf{n})$$
$$\mathbf{U}^\dagger\mathbf{y} = \mathbf{\Sigma x} + \mathbf{U}^\dagger\mathbf{n}$$

Let $\mathbf{y}^* = \mathbf{U'y}$ and $\mathbf{n}^* = \mathbf{U}^\dagger\mathbf{n}$;

$$\mathbf{y}^* = \mathbf{\Sigma x} + \mathbf{n}^* \tag{6}$$

Figure 4 shows the application of (6), illustrating the decomposition of **H** into *k* subchannels with gain, σ.

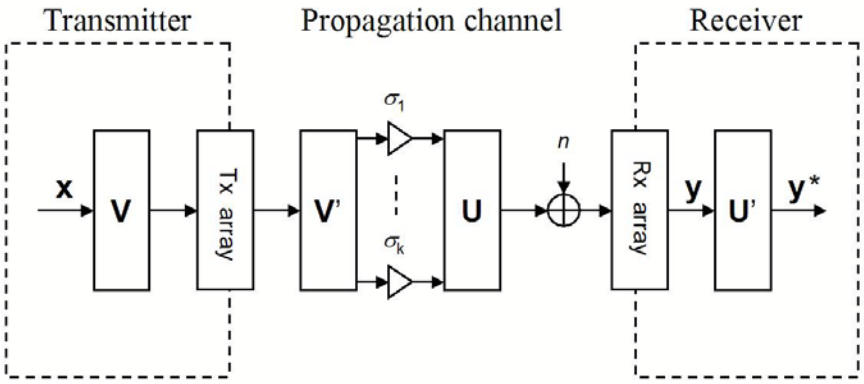

Figure 4: Subchannel decomposition of H

2.5.1 Sub channel redundancy

Consider an $n_T = 2$, $n_R = 3$ MIMO system as follows:

$$\begin{bmatrix} y_1 * \\ y_2 * \\ y_3 * \end{bmatrix} = \begin{bmatrix} \sigma_1 & 0 \\ 0 & \sigma_2 \\ 0 & 0 \end{bmatrix} \begin{bmatrix} x_1 \\ x_2 \end{bmatrix} + \begin{bmatrix} n_1 * \\ n_2 * \\ n_3 * \end{bmatrix}$$

In the above case of $n_R > n_T$, y_3 contains noise only. Similarly, for any MIMO system where $n_T \neq n_R$, $y_z : z > k$ take no part in carrying data. However, techniques such as choosing the best q x p system (where $q < n_R$ and $p < n_T$) from available array elements to exploit the extra spatial diversity available may be of benefit.

2.6 MIMO capacity

A significant determinant of MIMO capacity is power allocation at the transmitter. In the absence of channel state information (CSI) at the transmitter, [2] states that uniform power allocation across all transmit elements optimises channel capacity. In contrast, CSI at the transmitter permits greater capacity through a more efficient use of transmit power known as *waterfilling*. The benefit of waterfilling to systems with full rank channel matrices is, however, less apparent with increasing

SNR [33]. Due to the non-trivial requirement for feedback of channel knowledge to the transmitter to undertake waterfilling, it will not be considered further.

With regards to the propagation model presented in Figure 3, the information theoretic, or upper bound on capacity, C (bits/s/Hz) for a complex AWGN MIMO channel under conditions of equal transmit power is: [2]

$$C = \log_2\left[\det\left(\mathbf{I}_{n_R} + \frac{\rho}{\mathrm{n_T}}\mathbf{H}\mathbf{H}^{\dagger}\right)\right] \tag{7}$$

where $\mathbf{I}_{\mathrm{n_R}}$ is an n_R x n_R identity matrix, ρ is the signal to noise ratio (SNR), n_T is the number of transmit antennas, **H** is the normalised (unit variance, zero mean) channel response matrix and $(\cdot)^{\dagger}$ denotes conjugate transpose**.**

Calculation of capacity using (7) requires the following assumptions:

- *Propagation channel is sufficiently narrow band to be flat fading*. Flat fading describes a channel where the signal bandwidth is less the minimum channel bandwidth that exhibits constant gain and linear phase.
- *No channel knowledge exists at the transmitter*. Under these conditions, the requirement for feedback is excluded and equal transmit power is applied across all transmit elements.

The capacity (bits/s/Hz) for n x n MIMO systems with increasing SNR is shown in Figure 5, clearly demonstrating the linear increase in capacity with the number of antenna elements [2]. The n = 1 case is equivalent to the Shannon limit, (1)

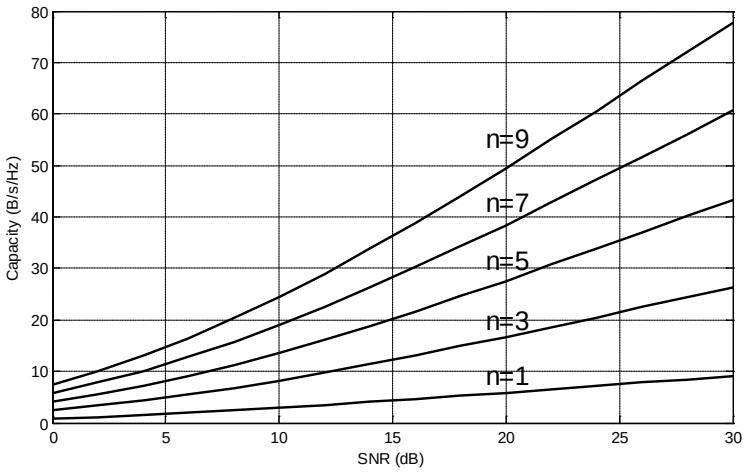

Figure 5: Capacity v SNR for various n x n MIMO systems

Received SNR is of critical importance to MIMO capacity. For example, consider a hypothetical 3 x 3 MIMO communication system transmitting with a 10 MHz bandwidth. With reference to Figure 5, the 1:1 gradient of the *n = 3* case (for SNR greater than 12 dB) shows an additional 30 Mbits/s of capacity is achievable by doubling received signal power.

2.7 Normalisation

The variation of measured SNR with the spatial characteristics of the propagation channel requires some form of normalisation for meaningful comparison of MIMO channel gain between separate locations. The choice of normalisation technique determines whether the calculated capacity is a relative or absolute measure. Derivation of the normalisation factor, η for each channel realisation allows calculation of absolute capacity for the given propagation environments and hardware configurations. The use of a single value of η with multiple channel response matrices allows for relative comparisons between environments and hardware arrangement.

The usual objective of normalisation is to scale the entries of the channel response matrix to have zero mean and unit variance. The n_R x n_T x f channel response matrix, **H** is normalised by division with the normalisation constant, η:

$$\eta = \sqrt{\frac{\sum_{i}^{n_R}\sum_{j}^{n_T}\sum_{k}^{f}|\mathbf{H}|^2}{n_R \cdot n_T \cdot f}} \tag{8}$$

SUMMARY

Chapter 2 has summarised the need for, and basic operation of multiple input multiple output communications systems. The behaviour of *line of sight* and *non line of sight* propagation conditions has been compared through observation of measured data. The frequency response of a NLOS channel typically exhibits lower average receive power with a greater number of multipath induced fades. The increased complexity of multipath interactions, in conjunction with typically greater displacement between users increases delay spread in NLOS circumstances. The coherence bandwidth of measured channels decreases with transition from LOS to NLOS, although this may be alleviated with techniques such as the use of multiple sub-channels. The following topics are presented: a generic MIMO propagation model (with relevant assumptions regarding usage), singular value decomposition of a MIMO channel into the into min(n_R,n_T) subchannels, equal power MIMO capacity and propagation channel normalisation techniques. A detailed discussion of the development and operation of the measurement system follows in Chapter 3.

Chapter 3

HARDWARE DEVELOPMENT AND OPERATION

PREFACE

Chapter 3 consists of a discussion of the practical components to this project required to achieve the channel characterisation objectives listed in section 1.3, *Contribution of the thesis*. The measurement apparatus utilised a combination of commercially sourced and purpose developed hardware for data gathering, with task specific software written for system control. The development and implementation of the measurement system is presented, including software operation, measurement protocols, antenna development and relevant antenna theory. The system uses a synthetic transmit array to sequentially measure the individual channels between each transmit and receive element pair of a user defined MIMO system. The chapter concludes with a discussion of calibration techniques employed to isolate the propagation channel response from that of the hardware in the measured data.

The target accuracy for the measurements is –35 dB, sufficient for 4G wireless systems. The calibration method and precautions used to achieve this accuracy are also described in this chapter. The gathering of large quantities of propagation channel measurements necessitated the design and development of several items of automated transmitter and receiver hardware. Purpose specific software was written in the Labview development environment to undertake system automation and data gathering. Complete computer control of the measurement system allowed channel measurements to be taken late at night, free from human intervention and interference. Computer automation also relieves human operators of the drudgery of manual control while reducing the possibility of operator error affecting the data.

3.1 Development goals

Prior to commencement, several goals for this project were set under the global intention of channel measurement:

- *To cost effectively and quickly develop a hardware solution to characterise a typical indoor MIMO environment in the 2.4 to 2.5 GHz ISM band, using omnidirectional, multiple element arrays.* The measurement hardware is a multiplexed system using a single transmit element attached to a horizontally mounted x-y positioning system, with an RF-switch addressed, fixed receive array.
- *Hardware and software to be readily reconfigured for other measurement campaigns.* Receive array composition is readily changed, as is the transmit element. The software allows alternative transmit-element locations and different inter-element separation on the x-y table to that used in the main measurement program.
- *Hardware to have measurement accuracy commensurate with current- and future indoor-wireless applications.* A common figure of merit for the waveform accuracy of wireless systems is the error vector magnitude (EVM), providing a measure of the difference between the desired and received magnitude and phase. The IEEE802.11a wireless LAN standard requires an EVM better than –25 dB. The accuracy of

any channel measurement data should be better than this to avoid dominating the performance of the link. A 6 dB margin is proposed, giving a channel accuracy requirement of -31 dB. Future uses of the measured data might require even greater accuracy and so the target accuracy for the equipment is set at –35 dB. This can be obtained if the accuracy of the three constituent parts of the measurement equipment, the mechanical sub-system, the electronics sub-system and the measurement SNR each meet an accuracy requirement of –40 dB (1%).

- *To conduct further measurements with arrays of different composition to the standard omnidirectional.* Secondary measurement programs were undertaken. Data were gathered with directional receive elements or a dual polarised patch transmit element, using some of the original transmit locations. The use of several different antenna element types at the transmitter and receiver was intended to compare the performance of MIMO systems utilising various array structures.

3.2 Hardware description

The measurement system comprises a mobile transmitter, stationary receiver, network analyser and personal computer (Master PC) for system control and data storage. In the interests of minimising temporal and fiscal expenditure, the channel measurement hardware was developed as a multiplexed system, sequentially measuring each h_{ij} individually. The desirable alternative of sampling the full MIMO channel response instantaneously represented an unacceptable increase in hardware development cost and time.

The network analyser transmits a swept carrier from 2.3 GHz to 2.5 GHz and returns the complex transfer function of h_{ij} to the Master PC for storage and future offline analysis. See Figure 6.

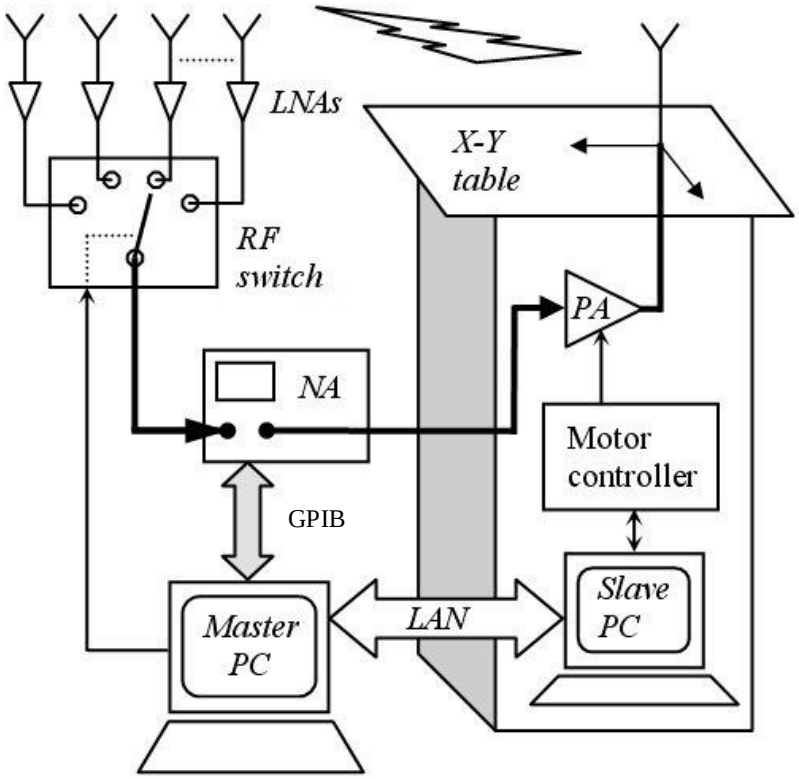

Figure 6: Measurement apparatus showing connection to the Network Analyser (NA). Dark lines show the RF signal paths.

The Master PC controls the movement of the antenna at the transmitter and the action of the RF switch at the receive array, in addition to controlling the operation of and storing data from the network analyser. At a given transmit table location, the x-y positioning system moves the transmit element to the first selected position. From the transmit element, the network analyser measures n_R complex frequency responses, multiplexing each receive array element with an RF switch. The transmit element is moved to any subsequent locations before the channel is sampled again to each receive element; fully characterising the n_R x n_T channel matrix, **H**, one column at a time.

3.2.1 Receiver

Figure 6 schematically shows an *n* element receive array (*n* = four or eight, for the omnidirectional and directional arrays, respectively) with associated low noise amplifiers and RF switch. The directional and omnidirectional receive arrays were used in separate measurement campaigns. Figure 7 shows that the omnidirectional array utilises four discone antennas, while the directional array employs eight dipoles.

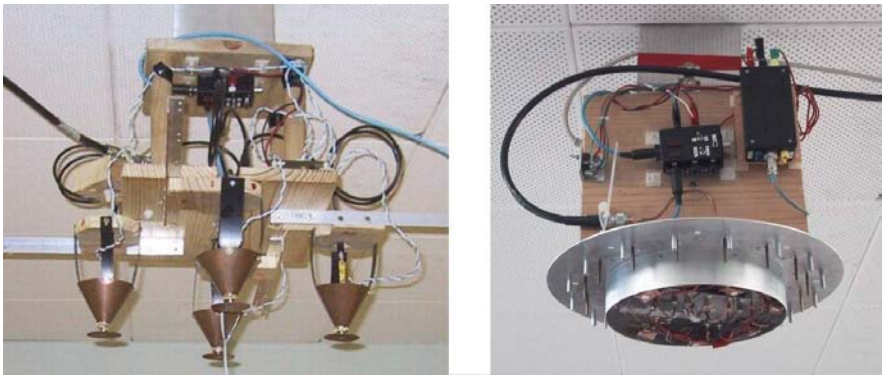

Figure 7: Four-element omnidirectional (left) and eight-element directional (right) receive arrays as installed to a laboratory ceiling.

The receive arrays were co-located to the same point on the ceiling of a laboratory at a height of 2.3m for each measurement campaign. The basic structure of either array is an RF switch multiplexing the amplified signal from each antenna to the network analyser.

Omnidirectional receive array

The four element omnidirectional array has a square pattern to the radiating elements (Figure 7, left). Each discone antenna attaches to a radial arm having manually preset locations along the length for adjacent element separation of one, two or four wavelengths at 2.45 GHz. Received signals pass from each antenna, through a low noise amplifier, through the active port of an RF switch and on to a network analyser. A block diagram of the omnidirectional array illustrating component locations is presented in Figure 8.

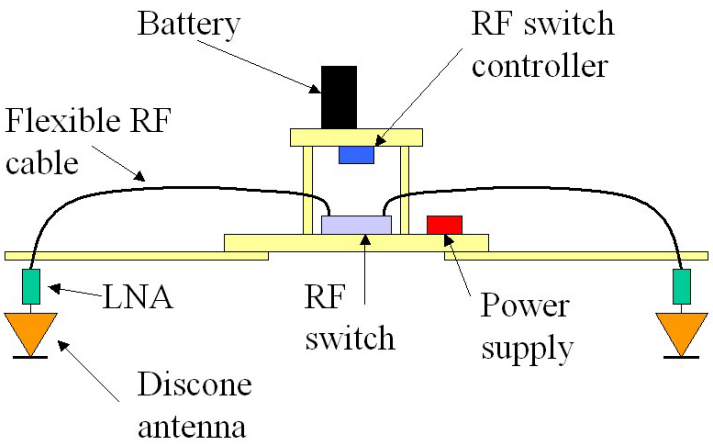

Figure 8: Block diagram of the omnidirectional array. With the exception of the discone antennas, labelled components are common to directional array also. Antenna and associated LNA location is adjustable to any of three locations, providing adjacent antenna displacement of one, two or four λ at 2.45 GHz

Directional receive array

The directional array is an eight-sector antenna. Eight dipole pairs tuned to 2.45 GHz are arranged circularly in the horizontal plane. The antenna elements are arranged with a radial distance of 150 mm, in front of an annular reflector of radius 120 mm (Figure 7 right). Each dipole element has a director element in front of it. As with the omnidirectional array, a network analyser samples received signals through a low noise amplifier and RF switch arrangement. The directional array structure (excluding low noise amplifiers and RF switch) was kindly provided by Stewart Jenvey of Monash University.

3.2.2 Ancillary Receive array hardware

Several items of hardware are common to both receive arrays shown in Figure 7: these are the power supply, an 8-port RF switch, an RF switch controller and low noise amplifiers.

Power supply

The power supply consists of a sealed lead-acid battery and LM78XX series linear regulators [34], supplying voltage to the RF switch, switch controller and low noise amplifiers. The use of a battery in place of a leaded power supply avoids complicating factors such as ground loops and RF noise being coupled into the receivers through a long power lead.

RF switch

A SP8T RF switch is used at the receive array to multiplex the amplified signal from each receive array element to the network analyser (See Figure 6). 50Ω loads occupy the four unused ports when used on the four element omnidirectional array.

The RF switch is composed of a Hittite HMC284MS8G SPDT switch multiplexing a pair of Hittite HMC241QS16 SP4T switches, thus providing the SP8T functionality required for use with the directional array (see Schematic 2 of Appendix A). The four-into-two arrangement ensures better insertion loss and greater overall isolation between ports than for a Hittite HMC253QS24 SP8T switch alone. Figure 9 shows the measured insertion loss and leakage characteristics.

The leakage traces occur in two distinct groups, as the isolation between RF switch ports attached to different SP4T switches is better than for the same device. Averaged (over frequency and each RF switch port) measured insertion loss through the active port and worst-case leakage to unused switch ports are -1.8571 dB and -34.7571 dB, respectively. The resulting average isolation of 32.9 dB is in agreement with published specifications for the HMC241QS16 and would ordinarily be considered more than adequate [35] to ensure minimal impact on data quality from the RF switch. However, as discussed previously in section 3.1, greater accuracy was sought for this work. Calibration procedures (to be discussed in section 3.5.1) were devised to counter errors induced by the electronic sub-system in the measured data.

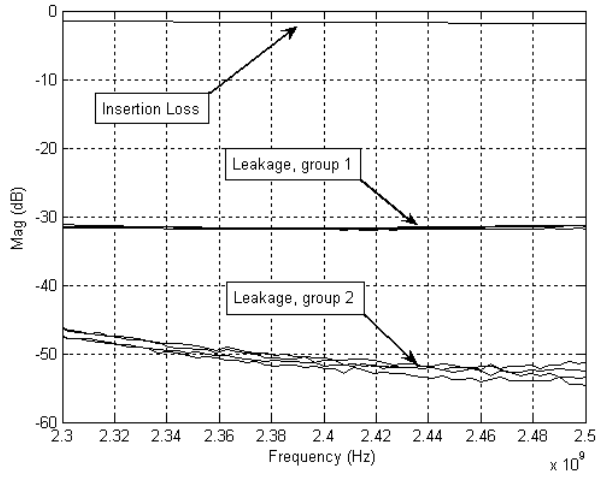

Figure 9: Typical RF switch insertion loss and leakage

The RF switch controller governs the operation of and powers the RF switch. Each of the three devices in the RF switch uses two control lines to determine switch position.

RF switch controller

An RF switch controller interfaces the parallel port of the Master PC to the RF switch. The switch controller is a generic device, able to operate RF switches in SP4T, SP8T or SP16T modes (see Schematic 3 of Appendix A). Switch banks A, B and C are three RF switch control ports. Banks A and B have drive capability for a SP8T switch, while bank C drives a SPDT switch. Control of SP4T and SP8T switches is available from bank A, while full SP16T functionality is realised when a SPDT switch on bank C multiplexes SP8T switches on banks A and B.

A three-way toggle switch determines the four, eight or sixteen throw mode of operation, with RF switch position and active RF switch bank shown on seven-segment displays. The first character displays A or B while the second shows the current RF switch position for that bank.

A choice of *clock* or *parallel* input modes provides flexibility in determining the active port of the RF switch. In the *clock* input mode, a falling edge on the C*lock*

IN input port increments the RF switch position by one. A reset action initialises the switch position when in clock mode.

The *parallel* input mode sets the RF switch position to reflect the first four bits of the parallel port connected to the controller. In parallel mode, the lower three bits of the input data nibble determine the switch position (1 to 8) and the MSB sets the active bank. For example, the nibble '0111' would specify bank A, position 8. A reset action will not be apparent in parallel mode if data remains at the input. In this case, the device will immediately return to the value stipulated by the input before the application of reset.

In the case of this work, the parallel port of the Master PC determined the position of a SP8T RF switch attached to bank A of the RF switch controller.

Low noise amplifiers

The low noise amplifiers are based on the Minicircuits ERA-3SM monolithic amplifiers [36] with a noise figure of 2.9 dB @ 3 GHz. This device is small, easy to implement, of low cost and has relatively low noise (see Schematic 4). Blocking capacitors at the input and output of the ERA-3SM isolate the DC supply and RF signal paths; a capacitance of 12 pF achieves a target series impedance of 5 Ω at 2.45 GHz. The Darlington pair configuration of the ERA-3SM requires a constant current source for stable gain, approximated by the series bias resistance. A parallel combination creates the desired resistance with reduced heat dissipation per resistor.

The 7 v supply allows some headroom with dropping battery voltage. With a 2.5 v drop across the linear regulator, a fully charged battery of 13.8 v can drop 4.3 v before the low noise amplifiers are affected. A relatively low bias voltage also assists further with heat dissipation in the bias resistance.

Series inductance in the bias circuit and a bypass capacitor at the supply input both aid RF rejection in the power supply. Four turns of 0.6 mm enamelled copper wire on a 3 mm mandrel form an air core inductor. Adjustment of inductor inter-winding separation while observing S21 frequency response on a network analyser is a successful technique to optimise amplifier gain.

*3.2.3 **Transmitter***

While a multiplexed transmit array could have been implemented in an identical manner to that at the receiver, a synthetic array generated with a single mobile element was chosen. The synthetic array possesses two significant attributes; excellent user definability and potentially large array size without complicated RF switching networks.

The dual axis antenna positioning system, or x-y table uses a rack and pinion drive system to horizontally locate the transmit antenna with a resolution of 0.1 mm. Software on the Master PC controls the antenna location on a 17 x 17 grid where the inter-positional spacing is usually predefined at 30.6 mm (corresponding to λ/4 at 2.45 GHz). The x-y table is mounted to a mobile cabinet housing a dual stepper motor controller, RF power amplifier, laboratory power supply and a personal computer (Slave PC) as shown in Figure 10.

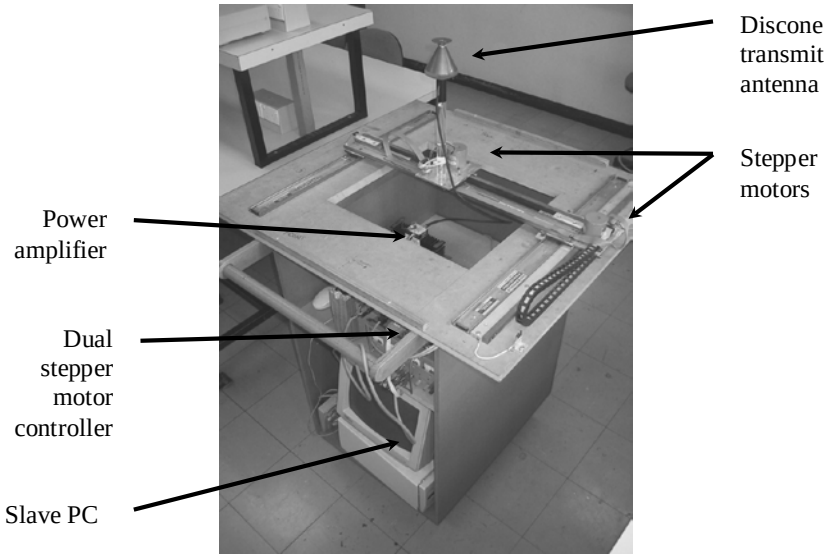

Figure 10: The transmit x-y table

The central item of hardware on the transmitter is the dual stepper motor controller, developed to accomplish the following tasks:

- *To move the transmit antenna by controlling a stepper motor for each of two horizontal axes.*
- *To switch supply voltage to the power amplifier and an optional pre amplifier*. The pre amplifier is occasionally necessary to ensure good SNR with long transmission distances.
- *To control a 2-way RF switch for use with a dual polarised antenna or a two-element array*.

The Slave PC in this installation is simply an interface between the dual stepper motor controller and the local area network (LAN) connection to the Master PC. Neither parallel nor RS-232 serial links are reliable over the potentially long distances between transmitter and receiver required for this project. Unlike other potentially faster methods, a LAN link posed a minimal time and financial burden to implement. The dual stepper motor controller decodes serial control information sent by the Slave PC to drive the two stepper-motors, one for each horizontal axis.

The dual stepper motor controller also receives data from the first two bits of the Slave PC parallel port to control relays used to switch 12 V to the power amplifier and optional preamplifier. A MAX232 serial transceiver converts RS232 line levels from the Slave PC into TTL levels for a PIC16F84 micro-controller. The PIC provides control and distance counter signals to each motor controller block. These consist of an L297 stepper motor controller driving an L298 H-bridge stepper motor driver.

The PIC reads in serial data by the byte, which may be either a counter value used to control the distance of movement of either motor, or a control byte that dictates the operation of the stepper motor controllers. Error correction is employed, where the transmitted data byte nibbles are swapped, transmitted and then retransmitted in original form. The first byte received by the PIC has the first and last four bits swapped back and then compared with the second byte. The PIC then replies to the Slave PC to indicate whether the transmission was successful, allowing for a retransmission if necessary. Each bit of a command byte maps to a control input of the L297s; direction, enable, and clock signals are motor specific, with speed and reset being ‘global’ commands. A counter value is a 15-bit number (bit 7 of the upper byte is not used) sent as two bytes, allowing for a maximum count of 32767 clock

cycles. Alternatively, a more common technique such as an 8-bit CRC could have been employed.

Displacement accuracy

In the case of measured data generated by the hardware described in this thesis, EVM is exacerbated by phase errors arising from inaccurate transmit element positioning. In the interests of maximising data quality, an EVM of -40 dB was desired in the measured data, corresponding to a phase error of 0.01 radians or a displacement error of 0.0016 λ. A 2.45 GHz carrier has a wavelength of 122.45 mm, so the x-y table should ideally exhibit positional resolution of 0.196 mm or better. The stepper motors are 1.8°, 200 step units that in conjunction with a drive pinion of diameter 37.8 mm, result in 648 clocks/λ (at 2.45 GHz). This equates to 0.189 mm of antenna travel per output clock (in full step mode) and is equivalent to an EVM of -40.3 dB. With the speed set to half step mode, this resolution increases to 0.094 mm/clock. Both full and half step modes have sufficient resolution to achieve the desired positional accuracy.

3.2.4 Network Analyser

The network analyser (HP8753C with the HP85047A S-parameter test set) measures the forward transmission coefficient of the measurement apparatus and wireless channel by driving the power amplifier on the transmit table and then measuring the channel response from the RF switch. The transmit power, IF bandwidth, and signal averaging functions were adjusted to give the target SNR of 40 dB. The noise floor was measured before and after each series of measurements to confirm the SNR requirement was met. Measurements are sent in complex notation back to the Master PC for observation and storage. Calibration of the network analyser and the RF cables linking it to the rest of the hardware is conducted prior to each measurement run to remove the behaviour of these items from the channel measurements.

3.2.5 Master PC

The Master PC automates the operation of the entire measurement apparatus and saves the results of any measurement data from the network analyser. Software written for this work governs the time of the first measurement, controls all relevant network analyser settings, selects the current RF switch position and determines all actions of the transmit table. The Master PC is linked to the network analyser with a GP-IB interface, to the RF switch with a parallel cable and to the Slave PC with the local area network.

3.2.6 Measurement Software

A purpose-programmed virtual instrument (VI) within the *Labview* development environment automates the measurement system. The operator is presented with a graphical user interface as shown in Figure 11, which allows control of transmit antenna locations, number of RF switch ports and network analyser measurement parameters.

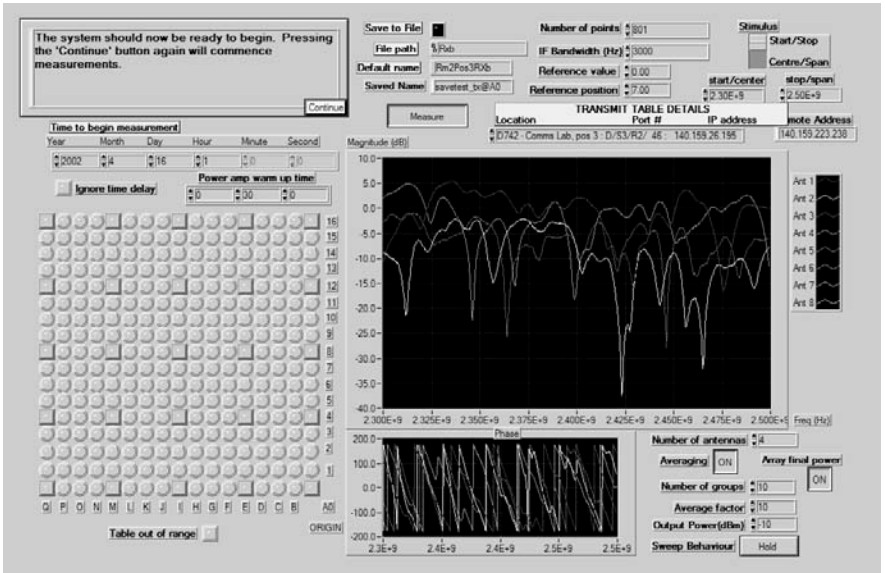

Figure 11: Virtual Instrument control panel on the Master PC showing typical magnitude and phase results of an indoor channel measurement

The VI also provides a checklist of tasks to ensure correct initialisation of the hardware, reducing the risk of erroneous data due to operator error. A time and date delay feature allows early morning measurements to ensure a static channel, free from human interference. Additionally, thermal equilibrium of the transmit power amplifier is assured prior to data gathering with a pre-measurement warm up period.

The user can select any number of transmit antenna positions up to 289, from a 17 x 17 grid. At a software level, the contents of each column of the input grid are examined sequentially for selected transmit antenna locations. This results in the transmit antenna moving in a scanning pattern over the possible range of movement. In response to one or more positions in column *A*, the antenna will move along the vertical axis to these sequentially, before moving back to the horizontal axis after measurement at the last location in the column. Movement is then initiated in the horizontal axis to the next column (B to Q) containing a transmit position so that a vertical cycle can be repeated. This regimen ensures that desired movement in each axis occurs in one direction only; the vertical axis is reset to a home position for each new column. The direct benefit is that backlash in the stepper motor drive pinion relative to the rack is avoided by not making repeated movements back and forth without mechanically resetting to a known position.

While the software allows for up to 289 user-definable transmit antenna locations, measurements with the omnidirectional receive array used a preset star pattern of 65 locations. The number of transmit element locations was reduced to 33 for directional array measurements to reduce the overall measurement time for a given table location.

The most important user defined settings of the VI are as follows:

- *Checklist*. The top left corner of the VI has a frame containing a text message and a CONTINUE button. Measurement will not begin until a series of initialisation steps have been carried out to reduce the possibility of a set-up error rendering a data set useless. The user is stepped through the initialisation process, ensuring each item of hardware is connected and calibrated as necessary to guarantee correct system function.
- *Counts per movement*. Each square or circle on the transmit pattern in the lower left of the VI represents a transmit antenna movement step of $\lambda/4$ at 2.45 GHz. The number of clock cycles or motor steps required for this distance is

entered here. There is no hardware requirement to limit this distance to λ/4 since the number of cycles per movement is user definable. The minimum movement corresponding to one cycle is 0.094mm (or 8.36×10^{-4} λ @ 2.45GHz), for the benefit of any future use of the hardware.

- *Measurement type*. Channel measurements are taken with the default GATHER DATA setting, while CALIBRATION is used to measure the hardware frequency response alone. The application of hardware calibration data to a measured channel response isolates the actual channel response from the measured data that also includes hardware influences. Refer to section 3.5.1 for full description of this process.
- *Save to file*. While enabled by default, file saving is an optional function to facilitate error checking and system demonstrations.
- *Time to begin measurement*. Allows date delay and time delay to start of measurements.
- *Transmit table details*. This is a pull-down menu of transmit table locations, listing the IP configurations for network ports near each table location.

A test run measurement is taken at the end of the set-up process, allowing confirmation that a channel measurement has in fact been taken and saved to the correct location with the correct naming convention. The gain and phase responses of the propagation channel between a given transmit element location and each receive antenna is displayed for demonstration and error checking purposes.

Data storage

The *Save to file* check box enables the *File path* and *Default name* fields, containing the intended destination of saved data and file name information, respectively. The file names of saved data follow a general naming convention describing all aspects of the measurement to which the file applies. A given file name consists of two parts; the contents of the *Default name* field and an automatically generated suffix containing the transmit element location and selected number of receive elements. For the purposes of this project, *Default name* contains a receive array description (when the omnidirectional array is not used), room number, position number and omnidirectional receive array inter-element separation, where applicable.

DirectionalRm1Pos1_tx@E4_8ant and *Rm1Pos1Rxa_tx@A0_4ant* are examples of saved file names.

3.2.7 Antenna development

This work utilised a combination of purpose developed and externally sourced antennas, all based around conventional designs. The discone and dual polarised patch antennas were developed as part of this work, while a colleague donated the circular dipole array.

Discone

The discone topology has the beneficial characteristics of very wide bandwidth, omni-directionality, modest cost and simplicity of fabrication. The discone antenna developed for this work and corresponding radiation pattern is presented in Figure 12.

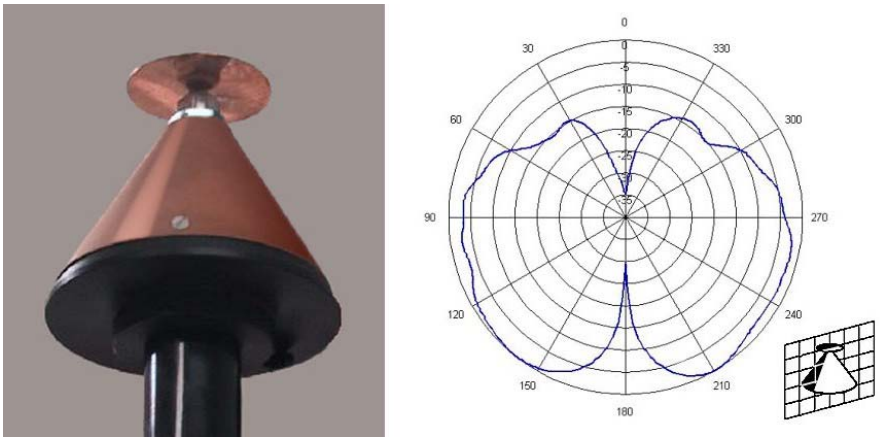

Figure 12: Discone antenna and measured vertical radiation pattern

Measurements were taken through vertical and horizontal planes in an anechoic chamber and clearly demonstrate the characteristic lobed radiation pattern. Rotation through the vertical plane reveals strong nulls directly above and below the element and a horizontal cut clearly shows the omnidirectionality of the design with uniform power over azimuth.

Scattering parameters were measured for this design on the HP8753C network analyser, revealing an exceptionally wide –10 dB bandwidth from 1.04 GHz to beyond 6 GHz (the upper frequency limit of the machine), ensuring a flat frequency response in the band of interest. The cone was formed over a mandrel while spinning on a lathe from a flat disc of 0.5 mm copper, with the apex dimensions to suit an N-type RF connector (Huber + Suhner part number 22_N-50-0-2/133_N). Figure 13, with dimensions in mm, shows this was utilised as it forms part of the structure by joining the cone and top disc together, in addition to providing electrical connection. A copper rod soldered to the centre conductor of the N connector facilitates tuning, where the top-to-cone clearance is adjusted for optimal standing wave ratio on the network analyser. The dimensions shown were found to provide good (-20 dB) matching at 2.45 GHz in addition to the previously mentioned wide bandwidth.

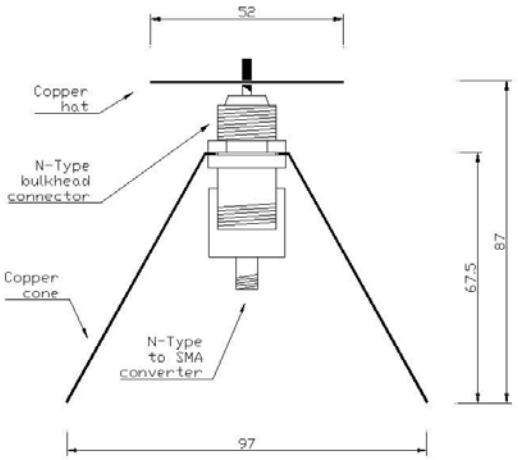

Figure 13: Discone element cross-section

Development of the discone dimensions was an iterative process, beginning with the following initial approximations:

Disc diameter: 0.17 λ

Cone side length: 0.25 λ

Cone apex angle: 25º - 40º, 30º used

where λ = wavelength at lowest operating frequency, arbitrarily defined here as 1 GHz to ensure that the operating frequency was well in-band. The initial conditions

above call for disc diameter and cone length to be 51 mm and 75 mm, respectively. Trial and error while observing standing wave ratio on a network analyser resulted in the final dimensions shown in Figure 13.

Circular dipole (directional) array

The circular dipole or directional array represents the type of installation that may be more typically employed as a directional, multiple element base station array in a wireless communication system. The measured radiation pattern of the circular dipole array in the horizontal plane, Figure 14, indicates the directionality of one element.

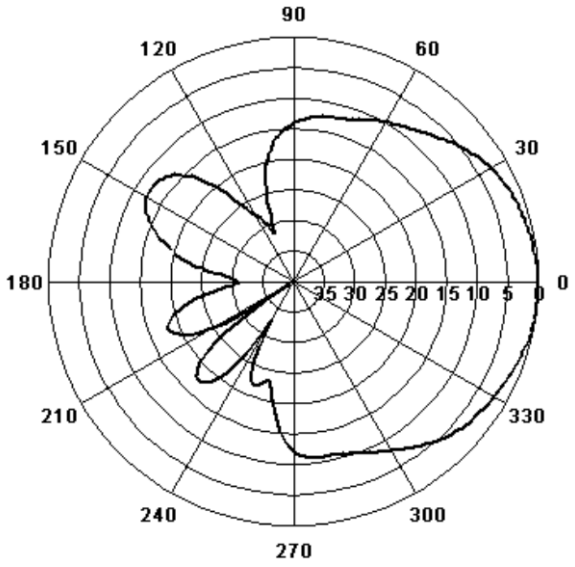

Figure 14: Radiation pattern of a single sector from the eight sector directional array (Figure 7 right)

The standard measurement bandwidth of 200 MHz is restricted to the operational bandwidth of 85 MHz for data analysis of MIMO systems using the directional array. The circular dipole array used the same power supply, RF switch, switch controller and low noise amplifiers as the omnidirectional array.

Figure 15 shows the frequency response over the measurement bandwidth of the mean return loss of all eight elements and the worst-case cross coupling. The –10 dB operational bandwidth of 85 MHz is indicated. The solid trace of Figure 15

charts the mean return loss over all eight elements of the dipole array, while the dotted trace presents the worst case (adjacent element) cross coupling between dipole array elements to be an average of –31 dB over the operational bandwidth. Typical cross coupling between non-adjacent elements is –50 dB.

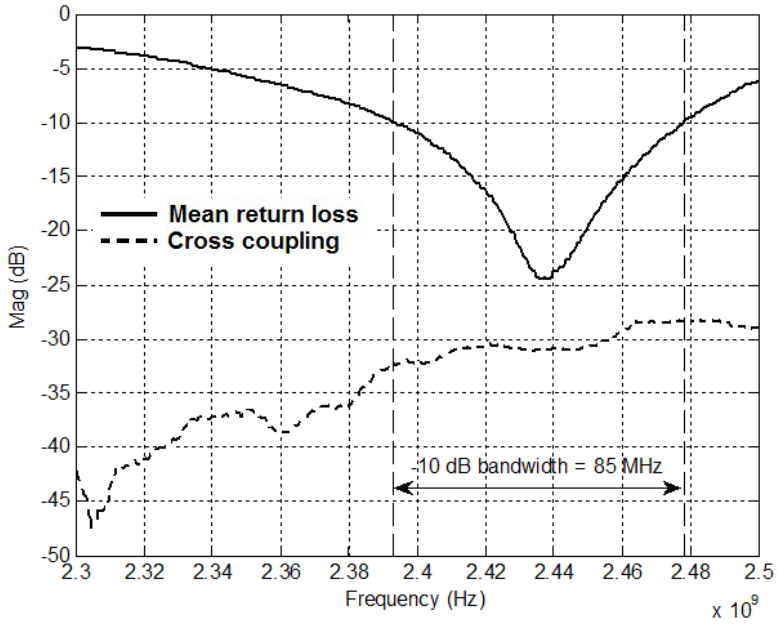

Figure 15: Mean return loss and worst case inter-element cross coupling of dipole array (Figure 7right)

Dual polarised patch

Conventional designs of microstrip or patch antennas commonly call for the suspension of a rectangular conductor by a dielectric material over a ground plane. Benefits of this structure include straightforward fabrication, low mass, unobtrusive physical profile and relatively small cost. The inherent narrow bandwidth of this basic design is, however, a less desirable characteristic and physical size can be an issue in miniaturised applications. The microstrip antenna is typically λ/2 in length and operates in the fundamental resonant mode, the resonant frequency of such a structure being given by:

$$f \cong \frac{c}{2L\sqrt{\varepsilon_r}} \tag{7}$$

where c, L and ε_r are the speed of light, length of patch and relative permittivity of the substrate, respectively.

Strategies for array miniaturisation were examined in this work, including reducing individual element and overall array size. Equation (7) indicates that increasing ε_r is a viable approach to reduce the resonant length of the patch. Another common technique is the use of an edge-shorted half wave patch, creating a quarter-wavelength device with a 50% reduction in physical length. Inducing meandering surface currents of an excited microstrip antenna is another well-known and simple method of lowering the resonant frequency; or reducing patch size for a given frequency. Cutting notches of appropriate dimension and location into the edges or body of a patch increases the minimum surface current path length.

Accuracy, ease of and rapidity of manufacture were paramount for the measurement programs described in this project. A microstrip antenna made by machine, solely from readily available PCB substrates was more desirable than one requiring time-consuming sectional assembly.

Applying any of the above techniques to individual array elements may reduce overall array dimensions, but reducing the actual number of physical devices is also of benefit. A dual-polarised structure with sufficient isolation between polarisations would halve the number of antenna elements, potentially very useful in volume critical applications such as hand-held devices. An existing design [37] for operation at 1870 MHz was adapted to 2.45 GHz for this work as it had several desirable characteristics. It is a mass-producible design based upon a common PCB material (FR4), requiring no further construction work postproduction than simply installing connectors. Figure 16 shows the dual polarised patch antenna used for this work.

Figure 16: Dual polarised patch antenna - radiating patch and ground plane perimeter

The patch is fabricated from double-sided board with a ground plane on the reverse side. The outer edges of Figure 16 indicate the ground plane perimeter (refer to appendix C for dimensions) relative to the patch dimensions. This device is probe fed, as evidenced by the two regions of solder near the centre of the patch. Two short lengths of semi-rigid cable terminated with SMA connectors are soldered to the ground plane, with the centre conductor passing through the board to excite the patch.

The combination and arrangement of slots in the surface of the patch results in 16.8% miniaturisation from the length of 29.19 mm for f_c = 2.45 GHz, calculated with (7). Figure 17 shows the frequency response of the dual polarised patch used in this work. The solid trace of Figure 17 shows the antenna input matching, while the dotted line is the cross polarisation leakage. The -10 dB bandwidth of the dual polarised patch antenna is 53 MHz, centred at 2.452 GHz. The mean cross polarisation leakage over the operational bandwidth is –25 dB.

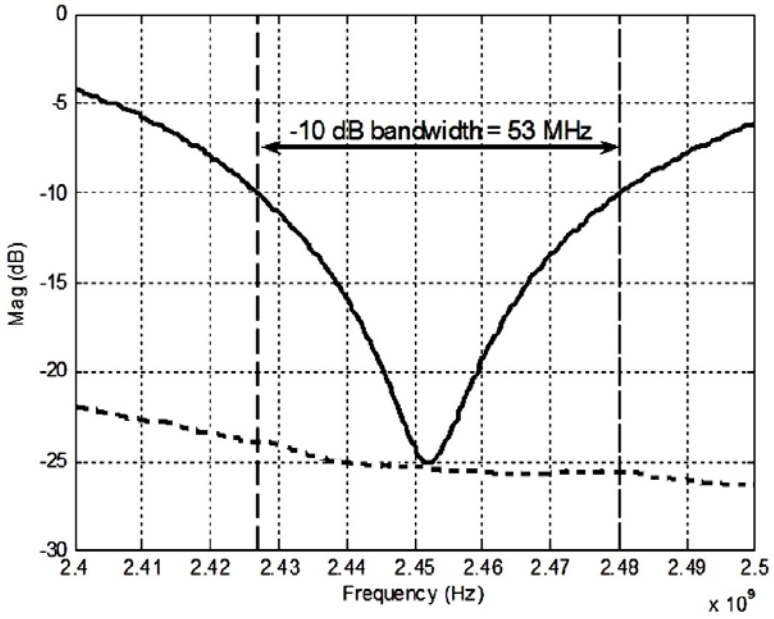

Figure 17: Dual polarised patch frequency response showing antenna input matching to 50 Ω and cross polarisation leakage.

3.3 Measurement programs

Following completion of the hardware, measurements commenced in January 2002. Three measurement programs were undertaken on the seventh floor of building D and the Footscray Park campus of Victoria University in Melbourne. The complete propagation measurement database created for this project comprises information from a primary and two secondary measurement programs. Each of the three campaigns occurred in the same propagation environment. Table 2 outlines the various transmit and receive architectures used in the three measurement programs.

Table 2: Measurement program details

Program	Transmit element	Receive array	Comments
A	Discone	Omni	Primary data set
B	Discone	Directional	Reduced Tx locations
C	Dual polarised Patch	Directional	One Tx location only

Program A included 23 individual transmit sites throughout the building, extensively characterising the propagation environment under a wide variety of line of sight (LOS) and non line of site (NLOS) conditions. Program A represents the main body of the measurement effort and constitutes a baseline for alternative hardware comparisons.

Program B was essentially identical to program A, with the exception of the receive array and was intended to allow investigation of any potential difference between directional and omnidirectional receive arrays.

Program C sought information about a more realistic choice of transmit antenna topology than the bulky discone type.

Figure 18 indicates the combination and location of transmit and receive arrays for each measurement program. For each measurement program, the receive array was installed on the ceiling (2.7m high, antenna feed points at 2.3m) of a laboratory. Measurements were taken with the transmitter moved to varying nearby locations on the same floor. With respect to the transmitter, a range of local environments was desired. Locations included a small office cubicle, larger

laboratories and a hallway, chosen to include a combination of LOS and NLOS scenarios.

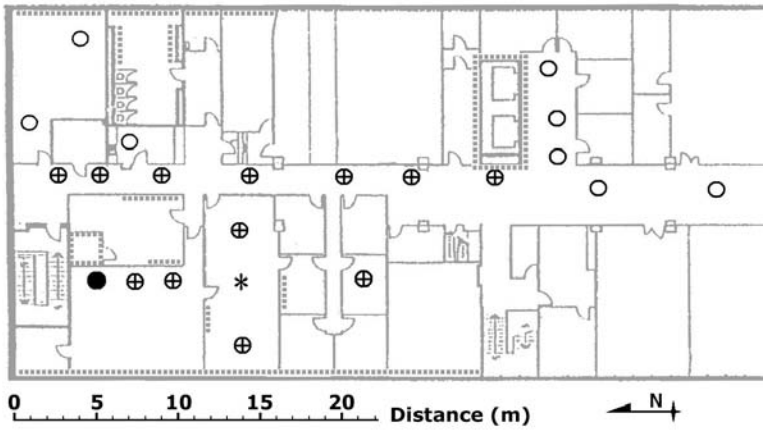

LEGEND

∗ Receive array, either omnidirectional or directional.

O *Omnidirectional* transmit array with *omnidirectional* receive array.

\+ *Omnidirectional* transmit array with *directional* receive arrays.

● *Dual-polarised* transmit array with *directional* receive array, in addition to the ⊕ combination.

Figure 18: Building D, Level 7 - Victoria University Footscray Park campus.

3.4 Measurement protocols

The ability to reposition the transmitter in an identical location for multiple measurement runs was a high priority. The actual transmit positions were accurately replicated in each program to constrain variables to the receive array topology only. Much of the propagation environment occurred in public areas and as such, the exact arrangement of small objects such as chairs and books not in the immediate vicinity to the transmitter was not under absolute control. Despite this, these relatively small items are assumed not to have any appreciable effect on the channel measurements. The close proximity of large reflectors or absorbers such as walls and doors to the transmitter is far more likely to have a significant impact.

An optical plummet[1] was adapted for use in the horizontal plane and allowed the transmitter to be repositioned with a very high degree of confidence between measurement programs. The optical plummet allowed small registration marks on adjacent walls to be telescopically observed while making fine adjustments to the transmitter location, ensuring accurate replacement of the hardware between measurement campaigns.

The ability to accurately reposition the transmitter table between measurement programs or in the event of a table disturbance during a program governed decisions on transmitter placement. This required unobstructed access to fixed reference points, usually a wall or other immobile object, from which the optical alignment device could be employed.

3.5 Data quality

Several initiatives aimed to ensure the highest possible quality of measured data: in the interests of aiming for the –40 dB accuracy of the mechanical subsystem, electrical subsystem and measured SNR mentioned in section 3.1

- *Regular network analyser calibration*. Factors such as ambient temperature and physical orientation affect the frequency response of the RF cables used to connect the network analyser to the transmitter and receive array. Calibration of the network analyser cabling occurs at the network analyser prior to the gathering of data at each transmitter location.
- *Power amp warm up.* Turning the power amplifier on 30 minutes before measurements commence ensures thermal equilibrium of the device.
- *Transmit table location accuracy*. The use of an optical plummet as described in section 3.4 allowed sub millimetre horizontal accuracy of the transmit table.
- *Transmit element location accuracy*. While the optical plummet provided precise spatial positioning for the array as a whole, relative

[1] An optical plummet is a surveying device, allowing the user to observe through an eyepiece, a magnification of a location in a direction along an axis perpendicular to that of the eyepiece.

spatial positioning accuracy between transmit array elements is of greater importance. The horizontal positioning system (section 3.2.3) accuracy is equivalent to -40.3 dB in full step mode or -46.3 dB in half step mode; both in excess of the -40 dB design goal.

- *Double shielded RF cable*. Cable leakage was minimised by the use of Huber + Suhner RG 214/U-01 double shielded cable, reducing the likelihood of direct coupling between the RF cabling attached to the network analyser.
- *Human and RF interference reduction.* Late night measurement times significantly reduce the likelihood of external interference from pedestrian traffic or other RF sources
- *Hardware calibration.* The application of ancillary hardware frequency response to measured data isolates the propagation channel from measured data, which includes influences from the electronic sub-system. This is described in detail in section 3.5.1.

3.5.1 Hardware Calibration

The ultimate goal of any measurement program is to produce data that accurately represents the channel response only and not a combination of the channel and measurement hardware. Hardware calibration measures were developed by observing the following frequency response representation of the measured channel response, $\mathbf{H}^{\Diamond}$:

$$\mathbf{H}^{\Diamond} = \mathbf{L} \,.\, \boldsymbol{\alpha} \,.\, \mathbf{H} \,.\, \mathbf{g} \tag{9}$$

where $\mathbf{L}$ is n_R x n_R the insertion loss and leakage matrix of RF switch, $\boldsymbol{\alpha}$ is an n_R x 1 frequency response vector of the low noise amplifiers, $\mathbf{H}$ is the n_R x n_T actual channel response matrix and $\mathbf{g}$ is the transmit power amplifier response vector.

Since the transmit array of this system is synthetically generated with a single antenna and power amplifier, $\mathbf{g}$ is in fact a scalar and may be grouped with the receive hardware resulting in a single term, $\boldsymbol{\chi}$, representing all non-channel based artefacts.

$$\boldsymbol{\chi} = \mathbf{L} \,.\, \boldsymbol{\alpha} \,.\, g \tag{10}$$

As dictated by (10), 'calibration' measurements taken of the measurement hardware may be used to correct the measured channel response to the actual channel response. These calibration data are then applied to each measurement file to remove all non-channel characteristics based on simple manipulations of (9) and (10):

$$\mathbf{H} = \boldsymbol{\chi}^{-1} \,.\, \mathbf{H}^{\Diamond} \tag{11}$$

Calibration measurements were taken with an attenuator in place of the channel to ensure appropriate signal levels at the receiver. A calibration matrix is created by sequentially connecting the PA-attenuator combination to each LNA input port in place of an antenna. An insertion loss measurement is then taken at that port of interest with leakage measurements made at the unused ports.

With respect to the hardware configuration described here, large transmitter to receiver displacements highlight the conflicting goals of achieving sufficient power at the transmit element (thereby ensuring adequate receive SNR) while reducing leakage from the transmit cable into the receiver network. A pre-amplifier was employed at the transmitter for the five Southern-most transmit locations (shown in Figure 18) to reduce output power at the network analyser while maintaining adequate transmit power. As a constant effect on all transmit measurements, a complex frequency response measurement of the pre-amplifier is used to scale the $\boldsymbol{\chi}$ matrix where appropriate.

Calibration procedure

A minor modification to the measurement apparatus was required to gather hardware calibration data. Figure 19 shows that the transmitting power amplifier is connected to the receiving low noise amplifiers through an attenuator (to model the losses of an actual radio path) rather than through free space.

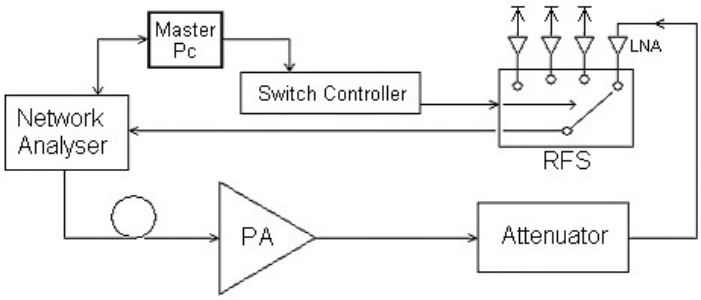

Figure 19: Hardware arrangement for receive array calibration

The attenuator depicted in Figure 19 (56 dB for omni array and 40 dB for directional array) is connected directly to the output of the PA and then routed to LNA 1, with the flexible shielded cable usually employed between the PA and transmit antenna. Ports 2 to *n*, where $n = 4$ for the omnidirectional array or 8 for the directional array, are terminated with their respective LNA - antenna combinations. An insertion loss measurement is taken through port 1, followed by leakage measurements through ports 2 to *n* (see Figure 9). Further noise reduction is achieved with a ten-fold average in each case. The full χ matrix is then constructed from insertion loss and leakage measurements for the other ports of the RF switch. Separate calibration data were gathered for each array. The resulting χ matrix entries are then scaled to account for the channel modelling attenuators so that χ accurately represents the hardware gain only.

A noise floor measurement was also taken with the power amplifier and RF feed cable disconnected from the network analyser. With no active transmission present, and an antenna driving each amplifier, all *n* switch positions were swept to show the measurement noise floor and to confirm a SNR of better than 40 dB required for the measurement SNR.

The internal calibration procedure of the network analyser was employed prior to the commencement of each measurement to exclude the frequency response of the RF cables from the gathered data.

SUMMARY

This system, entirely developed by the author, was intended for quick deployment, to cost-effectively generate information about the propagation channel behaviour and to provide insight into the physical constraints and requirements of MIMO measurement programs in general. This chapter provides detailed information on the development and use of a MIMO propagation measurement test bed. The -35 dB overall error specification can be obtained if each of the three major contributors (electrical sub-system, mechanical subsystem and measurement SNR) can be held to -40 dB.

Chapter 4

RESULTS AND ANALYSIS

PREFACE

Chapter 4 presents analyses of frequency and time domain responses, singular value decomposition and capacity of measured MIMO data for each of the three measurement campaigns. A review of the **MATLAB** analysis software written to examine the data is provided. The use of directional dipole receive arrays and dual polarised patch transmit arrays are compared to omnidirectional antennas in terms of capacity and singular values.

The measurement campaign undertaken for this thesis has characterised 4635 individual SISO paths at 34 physical locations to extensively describe the indoor propagation environment at the Footscray Park campus of Victoria University, building D, level 7. The resulting data encompass propagation conditions ranging from line of sight (LOS) to obstructed line of sight (OLOS) and non line of sight (NLOS) in a typical indoor office and laboratory environment.

4.1 Analysis software

Analysis of the measured data is facilitated with a MATLAB based graphical user interface (GUI), utilising a combination of nested functions, script files and

image files (see Appendix D). The main function *MIMO_analysis_win.m* creates the GUI (Figure 20) and calls the remaining sub-files as necessary.

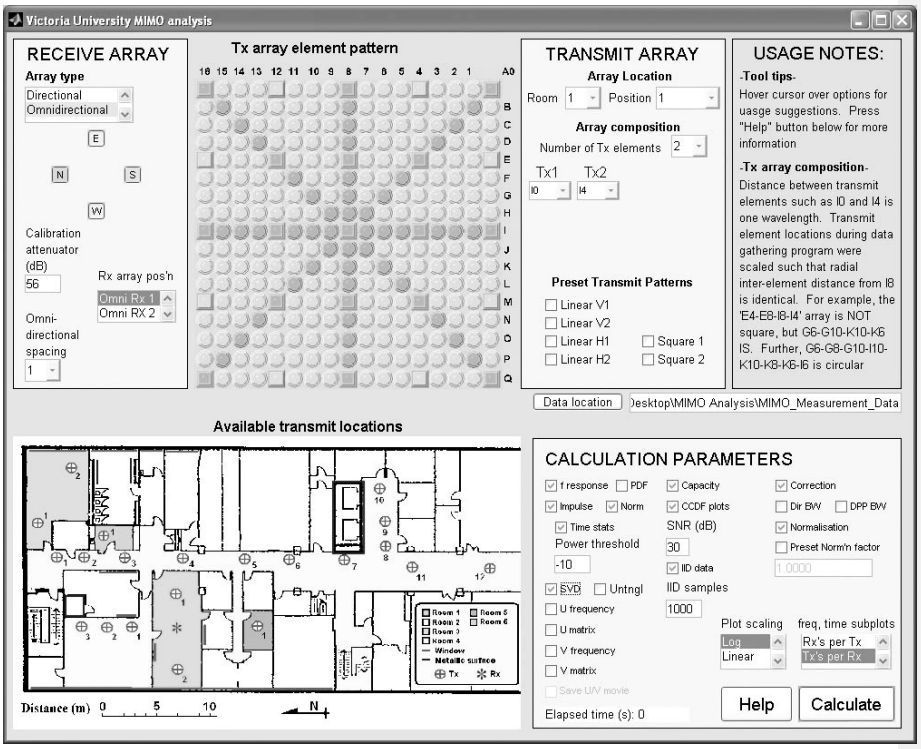

Figure 20: Measurement analysis GUI

Initial inspection of Figure 20 reveals two diagrams and three user input frames. The upper diagram is a representation of the 289 transmit element locations possible, with those actually used for the selected receive array type highlighted. The two diagrams are dynamically updated to indicate available choices of transmit element and transmitter location for a given *Array type*.

The first available choice from the *RECEIVE ARRAY* frame is between the directional and omnidirectional types. The *Array type* determines the arrangement of push buttons representing each available receive array element. An *omnidirectional* selection results in four elements appearing; Figure 20 shows the *E* and *W* elements selected. The *Calibration attenuator* field applies a fixed amount of gain to the calibration file use in the *Correction* process (see section 3.5.1), accounting for the

attenuator used during calibration measurements. Calibration gain correction is necessary for accurate observation of measured SNR. *Rx array Pos'n* allows selection of a dataset not considered in this thesis, created with an alternative omnidirectional receive array location. *Omni- directional spacing* is a pull down menu allowing selection of interelement separation at the omnidirectional receive array from one, two or four wavelengths.

Selection of *Directional* from *Array type* instigates several changes to the GUI. In the *RECEIVE ARRAY* frame, the number of receive elements is increased to eight, a *Preset Rx patterns* option appears and a *Use omni dir normfact with dir data* check box is added. Selecting *Preset Rx patterns* provides a pull-down menu to choose from *Sequential* and *Alternate*. The *Sequential* option generates eight MIMO systems, where a group of *Sequential group size* receive elements moves sequentially around the array. For example, the receive elements used for the first and second groups are Rx1 to Rx(*Sequential group size*) and Rx2 to Rx(*Sequential group size* +1). *Sequential group size* transmit elements are employed for *Sequential* calculations. *Alternate* creates two MIMO systems where four alternate receive elements (1,3,5 & 7 and 2,4,6 & 8) are used with up to four transmit elements. The *Use omni dir normfact with dir data* check box facilitates a fair comparison between receive array types by normalising the selected directional MIMO system with an equivalent omnidirectional normalisation factor.

Within the *TRANSMIT ARRAY* frame, pull-down lists contain available choices for transmit array location and array element composition. Room and position within a room are updated with *Array type* selection to reflect differences between measurement programs. Pull-down menus allow each transmit element to be selected from the highlighted locations of *Tx array element pattern.* Preset transmit array patterns are also available for linear, square or circular arrays with varying element numbers and separation. The maximum number of transmit elements is dictated by the selected number of receive elements.

Once the desired transmitter and receiver attributes have been selected, the *Calculation Parameters* frame contains the following analysis options:

- *f response*. A plot is generated for each transmit element, showing the frequency response from that element to each receive element. *PDF* creates a PDF plot of the frequency response data, although the number of samples is too small for any statistical significance.

- *Impulse*. An IFFT is applied to the selected frequency response data to provide a time domain plot. *Norm* and *time stats* are available options, normalising impulse response plot magnitude and calculating time dispersion statistics (excess delay and rms delay spread), respectively. The *power threshold* differentiates legitimate multipath signals from the noise floor (see Figure 2). *Power threshold* should remain constant for comparative purposes considering its influence on time dispersion statistics.
- *Capacity*. Ergodic capacity of the selected MIMO system is calculated using a fixed or measured SNR value. Capacity per frequency bin is plotted, with an average value included. If SVD is also selected, capacity is calculated with a successive removal of the smallest singular value until only the highest singular value, $\sigma 1$ remains.
- *SVD*. Singular value decomposition is carried out on the selected propagation channel and the resulting Σ matrix is plotted against frequency.
- *Untngl*. Singular values are 'untangled' by changing points of inflection between singular values to singular value crossings [38].
- *U frequency*. The entries of the U matrix are presented over the measurement bandwidth.
- *U matrix*. A bar chart is shown representing the average U matrix across frequency.
- *V frequency*. See *U frequency*.
- *V matrix*. See *U matrix*.
- *CCDF plots*. Complementary cumulative distribution functions are calculated for *Capacity* and *SVD*, if either or both are selected.
- *IID data*. *IID samples* of IID data are generated for comparative capacity CCDF and singular value plots.
- *Reduced BW*. The measurement bandwidth is restricted to match the operational bandwidth of the selected antenna types.
- *Correction*. Measured data are corrected for hardware artefacts as described in section 3.5.1.

- *Normalisation.* The calculation of capacity requires that measured data are normalised to zero mean and unit variance.
- *Preset Norm'n factor.* Fair comparisons between different MIMO systems requires identical normalisation factors. The normalisation factor of any previous calculation is pre-emptively placed in the *Preset Norm'n factor* entry field for use in subsequent calculations.
- *Plot scaling.* A choice of log or linear vertical scales is available for frequency response, Σ, U and V plots.
- *SNR (dB).* The SNR required by capacity calculations may be directly entered as a user-defined value, or calculated from measured data if the field is cleared.
- *IID samples.* Higher vales improve accuracy but increase calculation time.

The *"MIMO_Measurement_Data" path* button displays a dialogue box to select the location of the \MIMO_Measurement_Data directory. Hovering the cursor over objects within the GUI displays 'tool tips', providing helpful information about the function in question.

4.2 Channel stability

Of critical importance to switched antenna measurement campaign accuracy is the validity of the assumption of channel stability during measurements. Channel stability has been examined through analysis of the correlation between adjacent frequency response samples over time. A single transmit element was installed in a NLOS location within the same room as the omnidirectional receive array. The network analyser measured an 801-point channel frequency response from 2.3 GHz to 2.5 GHz at five minute intervals from 3:30 pm on a Friday afternoon to 2:05 pm Saturday. The total channel sampling period of almost 24 hours included episodes of pedestrian traffic and of total inactivity. Figure 21 charts the correlation coefficients calculated from adjacent time samples of the channel frequency response. The time

scale is of a 24 hour clock and shows a progression from the afternoon of one day to that of the next.

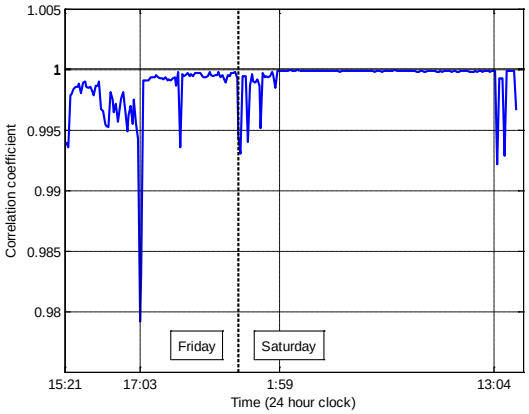

Figure 21: Correlation coefficients of adjacent propagation channel frequency response samples, measured at five minute intervals.

Pedestrian traffic was present in the room, except for the period from 1:59 am Saturday morning to 1:04 pm Saturday afternoon. Figure 21 shows a region of very high correlation of 0.9999 for the time of no pedestrian traffic, so the assumption of a static measurement channel during measurements is considered valid.

4.3 Indoor channel frequency response

The fundamental analysis of the measured data is observation of the channel gain frequency response. Amongst other things, a frequency response plot provides an indication of the extent of multipath in the measured channel and relative signal strength at each antenna.

Figure 22 has frequency response plots of the directional and omnidirectional arrays with the transmitter at the fourth hallway location from the Northern end. See Figure 18 for a floor plan of the measurement environment.

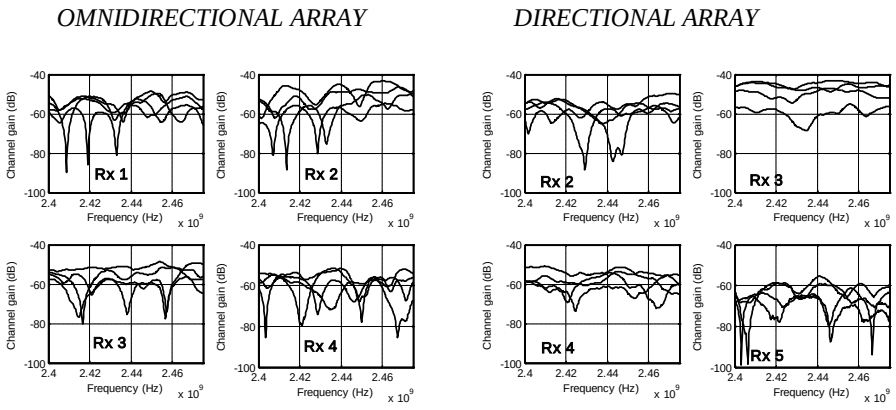

Figure 22: Four element frequency response comparison for omnidirectional (left) and directional (right) receive arrays with a transmitter at 14.3m along hallway.

A diagrammatic representation of the two receive arrays is shown in Figure 23, indicating the numbering convention used for the elements of each.

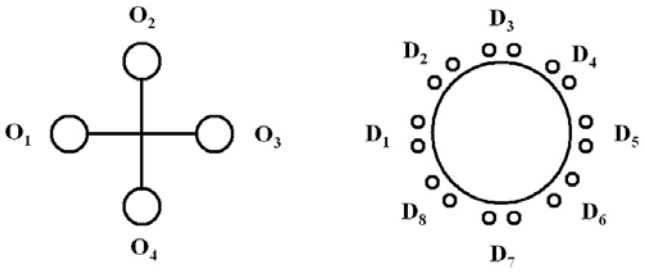

Figure 23: Receive array element numbering (plan view) of the omnidirectional receive array (left) and directional receive array (right). Element one faces North for either array.

For the channel under consideration, the transmitter is in a NLOS location east of the receive array; directly opposite receive element O_2 or D_3, as applicable.

4.3.1 Variation in measured channel gain

Two sources of non-uniform sensitivity over azimuth amongst individual elements of a circular or square multi-element array are *shadowing* by neighbouring elements and element directivity. The average (across all transmit elements and frequency) channel gains in dB measured at omnidirectional receive elements one to four are -55.6, -53.4, -56.4 and -58.3, respectively. Despite the omnidirectionality of the array, there is a progressive reduction in received energy across the array (from the element nearest to the transmitter, O_2 to O_4 on the other side of the array) as shadowing becomes an issue.

The directional antenna channel gains measured at receive elements two to five (see Figure 23, rhs.) are -57.3, -49.9, -58.1 and -65.4, respectively. The directional element radiation pattern (see Figure 14) is seen to have a more significant effect on channel gains than shadowing in the omnidirectional array. A difference of 15.5 dB exists between directional antenna three (pointing straight at the transmitter) and antenna seven (pointing the furthest away from the transmitter.

4.4 Indoor MIMO channel capacity

The information theoretic capacity as given by (5) is of particular interest in propagation channel evaluation, providing an upper bound to capacity in bits/Hz/s for a given MIMO system. Some preliminary assumptions are required when considering capacity calculated for data generated by this project. While the measurement hardware affords excellent spatial accuracy to the synthetic transmit array, data were gathered over a not-insignificant period, imposing some temporal assumptions: firstly that the physical characteristics of the propagation channel have not significantly changed between measurement programs; and secondly, that the propagation channel for a particular transmitter location is assumed stable during measurements. To this end, measurements were conducted automatically during the early hours of the morning to avoid human interference.

Following is an investigation of MIMO channel capacity dependence upon path loss, array element directivity, array element polarisation and channel correlation. Element directivity and polarisation are considered with and without path loss, using fixed and measured SNR.

4.4.1 Path Loss and array element directivity

Capacity may be examined using either a fixed SNR to examine the MIMO gain in isolation or measured SNR, which also includes the contribution of channel path loss.

The parallel measurement campaigns, programs A and B, allow investigation of the influence of array element directivity on capacity. Conventional MIMO theory often refers to optimum capacity being found in "rich scattering environments"; these being necessary to decorrelate signal paths at the receiver. An inference from this is that since an omnidirectional antenna will be sensitive to multipath over a greater azimuth than a directional counterpart, greater MIMO capacity will result. The validity of this proposition was tested by comparing the behaviour of the omnidirectional and directional receive arrays with an identical transmit array and propagation environment. The capacity of various MIMO systems was observed and compared to determine the benefits, if any, of using either receive array preferentially. Refer to Figure 24 for the single receiver and seven transmitter and locations referred to in the following discussion.

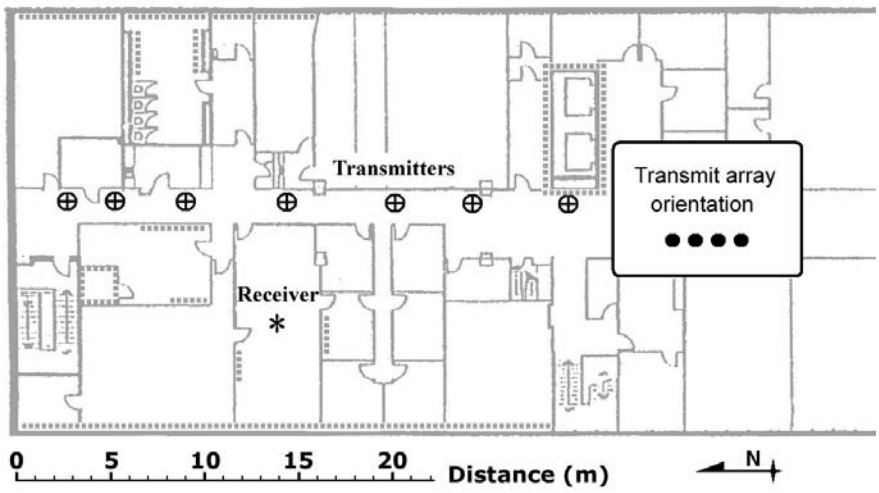

Figure 24: Locations of transmitters and receiver for examination of the influence of array element directivity on capacity. The linear transmit array using omnidirectional elements is arranged perpendicular to the central hallway for all seven locations.

Capacity calculated with fixed SNR

Figure 25 shows a capacity comparison (averaged across frequency) between several directional and one omnidirectional receive array, for a *fixed* SNR of 30 dB. For a particular transmit array, MIMO capacity for systems using the *directional* receive array was calculated with a normalisation factor from those using the *omnidirectional* array to allow fair comparison. The horizontal axis of Figure 25 represents distance from the northern end of the central hallway. The transmit array is comprised of four omnidirectional elements, linearly spaced 122.45 mm (λ at 2.45 GHz) apart, parallel to the long axis of the hallway.

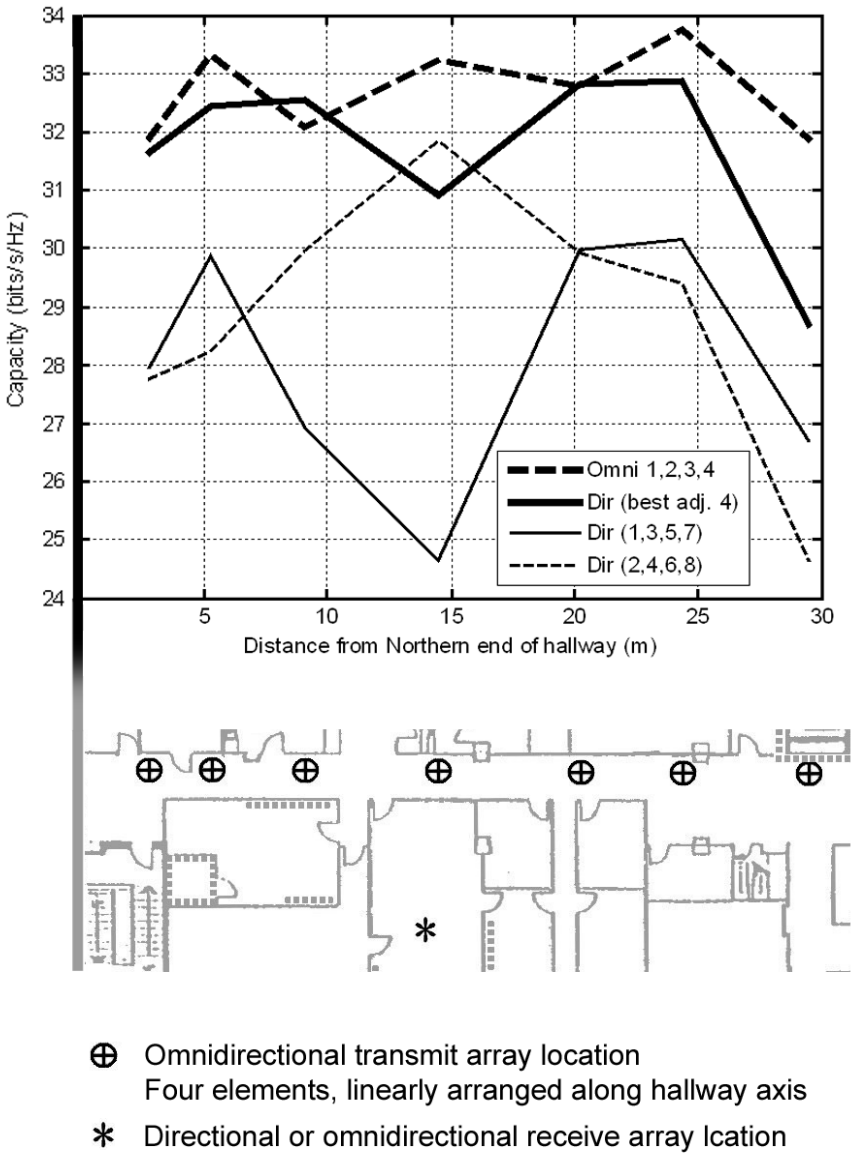

Figure 25: Capacity based comparison of directional and omnidirectional receive arrays (with *fixed* SNR = 30 dB) for varying transmit array locations along the central hallway of Figure 24. Linear transmit array, orientation as per Figure 24. Refer to Figure 23 (rhs) for directional array element numbering. The corresponding transmit array locations on an area plan are included for clarity.

DIRECTIONAL RECEIVE ARRAY

Consider a 4 x 4 MIMO system comprising the standardised omnidirectional transmit array introduced above, with directional receive array elements (Figure 23, right). The receive sub-array selection is of four adjacent elements, or either combination of four alternate elements.

- *Adjacent directional array elements*

For a given transmitter location, the four adjacent directional receive elements showing greatest MIMO capacity were chosen for 'best adjacent element' in Figure 25. The conspicuous trough in the adjacent element capacity at 14.5 m highlights the heightened sensitivity of directional elements to channel correlation. At 14.5 m, directional receive elements Rx7 to Rx2 (facing the opposite direction to the transmitter) show the greatest fixed SNR capacity, but this is still lower than the capacity at nearby locations along the hall. The capacity deficit at 14.5 m is due to a reduced opportunity to sample multipath arising from the relatively low displacement between transmitter and directive receive elements.

The classical MIMO requirement of de-correlated paths is well substantiated if SNR is fixed for adjacent element combinations of a directional array. With respect to Figure 25, greatest capacity is almost invariably found with the best group of receive elements facing directly *away* from the transmitter location.

- *Alternate directional receive elements.*

The capacity generated by either combination of four alternate elements (Rx1, 3, 5 & 7 or Rx2, 4, 6 & 8) is presented in Figure 25. The two alternate element combinations are shown, with one exception, to consistently exhibit reduced capacity compared to the best adjacent element combination of the directional array.

OMNIDIRECTIONAL RECEIVE ARRAY

Each of the four omnidirectional receive array elements are included in the 4 x 4 MIMO capacity comparison. The square (or circular) arrangement of omnidirectional elements (shown in Figure 23) is seen in Figure 25 to outperform all three directional array combinations by a minimum average of 1 bit/s/Hz.

Another noteworthy aspect of Figure 25 is that omnidirectional capacity is apparently unaffected by the transmitter location at 14.5 m, due to full azimuth sensitivity of each element, lowering overall channel correlation.

HALLWAY INDUCED WAVEGUIDE PROPAGATION

Although upon initial investigation, the reduction in capacity at the first and last transmitter locations shown in Figure 25 appears counter-intuitive (to an expectation of greater multipath with increasing transmitter to receiver displacement in a scattering environment), a rational explanation exists. Hallway structures in indoor environments tend to act as waveguides [32], necessitating a perpendicular arrangement of linear arrays to the corridor length for maximum MIMO capacity when the propagation is primarily parallel to the hallway. The result of rotating the first and last transmit arrays by 90° (becoming perpendicular to the hallway) is illustrated in Figure 26. Capacity is seen to increase at either end of the hallway compared to Figure 25 due to a greater ability of the transmit array to project along the hall.

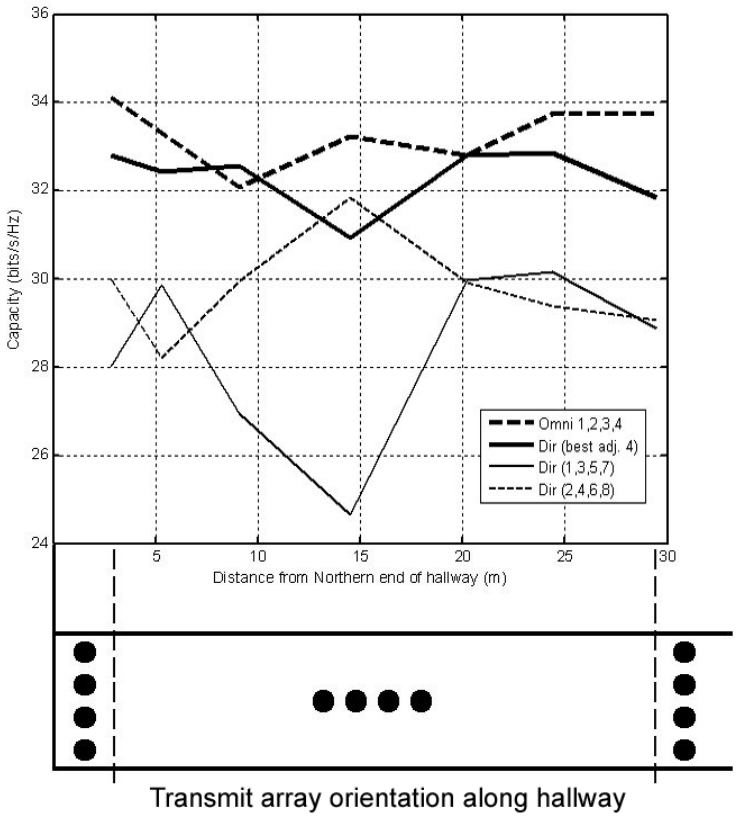

Figure 26: Capacity comparison – *fixed* SNR. Various receive array configurations with transmit array locations moving down the central hall for fixed SNR of 30dB. Transmit arrays at 2.8 m and 29.5 m are perpendicular to hall length, but parallel at locations between.

Capacity calculated with measured SNR

Figure 27 presents a capacity comparison between receive arrays for the transmit locations shown in Figure 24 using *measured* SNR. As in the last fixed SNR example presented above, the first and last transmit locations were examined with the transmit array perpendicular to the hall. The transmit and receive array configurations are identical to those discussed in the fixed SNR case.

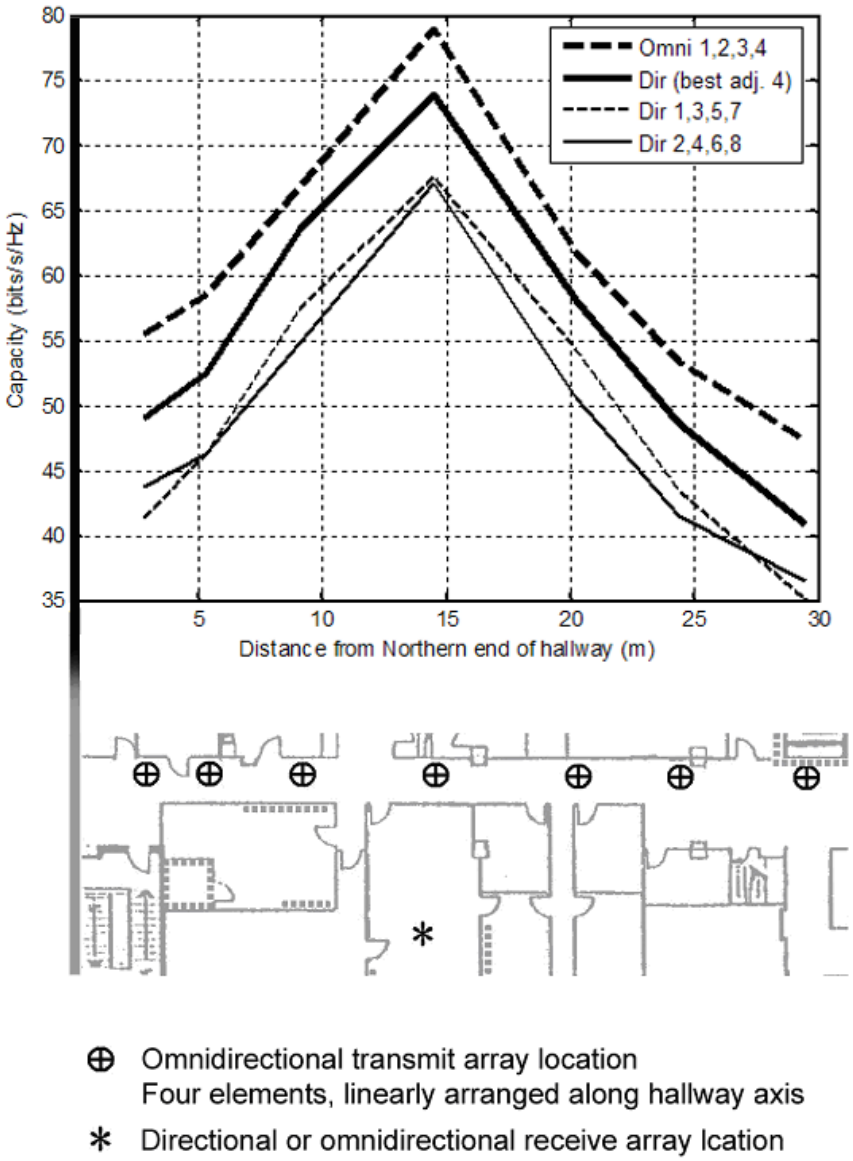

Figure 27: Capacity based comparison of directional and omnidirectional receive arrays (with *measured* SNR) for varying transmit array locations along the central hallway of Figure 24. Linear transmit array, orientation as per Figure 24. Refer to Figure 23 (rhs) for directional array element numbering. The corresponding transmit array locations on an area plan are included for clarity.

In the measured SNR case, the omnidirectional receive array consistently results in a mean capacity increase of 4.2 b/s/Hz over the best four-element directional sub array selection. The discrepancy between omnidirectional and directional arrays further increases in favour of the discone array to approximately 12 b/s/Hz when considering either combination of alternate directional elements.

The capacity improvement with an omni-directional array is due to full azimuth sensitivity at each antenna. Comparatively, the directional elements have a 60° -3 dB beamwidth and a group of four adjacent elements only covers 200° of azimuth.

4.4.2 Array element polarisation

The dual polarised patch discussed in section 3.2.7 saw service as a transmit array element at the location shown in Figure 28, allowing quantification of any possible benefit of employing multiple polarisations at the transmit array.

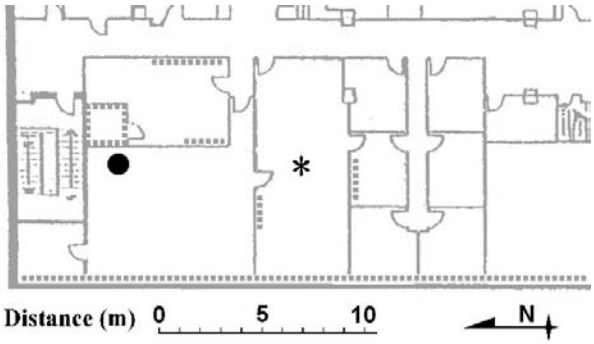

LEGEND

∗ *Directional* receive array.

● *Dual polarised patch* or *discone* transmit array.

Figure 28: Location of dual polarised patch or discone transmit array and directional receive array

Transmit array

Evaluation of systems employing multiple polarisations at the transmit array is possible since comparative measurements were taken (at the location shown in Figure 28) with a dual-polarised patch and with uni-polarised, omnidirectional transmit elements. Both systems under consideration used a combination of four of the available eight directional receive antennas. The transmit array comprised four omnidirectional (4 x 4), two omnidirectional (4 x 2) or two dual polarised patch (4 x 2_2) elements. Refer to section 2.2 for clarification of MIMO system size nomenclature employed in this thesis. Dual polarised patch elements were always mounted vertically and directed at the receive array during measurements.

Linear transmit arrays are composed of omni-directional elements separated by λ/4 (at 2.45 GHz), or by the use of both polarisations of two dual-polarised patch elements at the same displacement. See Figure 29.

Element type	Discone	Discone	Dual polarised patch (vertical)
Number of array elements	4	2	2
Number of antennas:	4	2	4
Transmit arrray composition and orientation	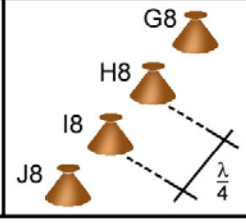	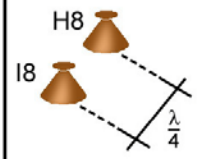	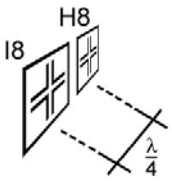

Figure 29: Transmit array comparison between omnidirectional discone and dual-polarised patch elements (see section 3.2.7 for a comprehensive discussion of antenna types), λ/4 separation at 2.45 GHz. Linear transmit arrays arranged broadside to receive array, with patch array elements facing receive array. Alphanumeric element labelling refers to locations on the transmit table, shown diagrammatically in Figure 11.

Patch antennas occupied the middle two omnidirectional transmit antenna locations (H8 and I8) to make comparisons as spatially fair as possible and measurement bandwidth was restricted to that of the dual polarised patch for all calculations. All channel matrices are normalised to the 4 x 4 reference system with omnidirectional transmit elements for either receive array configurations.

Receive array

Alternate and adjacent combinations of four directional receive antennas are examined. See Figure 30.

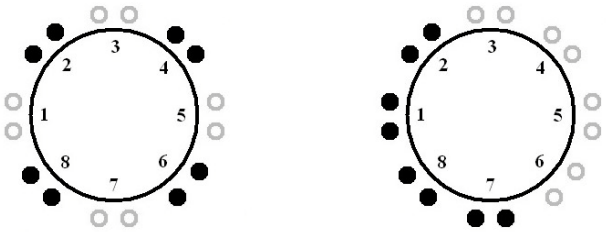

Figure 30: Directional receive array element combinations; alternate on lhs and adjacent on rhs.

Results

Table 3 presents a MIMO capacity comparison between omnidirectional and dual polarised patch transmit arrays with fixed or measured SNR

Table 3: Capacity comparison of omnidirectional and dual polarised patch transmit arrays.

MIMO system			Capacity (bits/s/Hz)	
Rx antennas	**Tx antennas**		**SNR=30 dB**	**Measured SNR**
Dir 2,4,6,8	Omni	G8,H8,I8,J8	28.19	52.4 @ 48.96 dB
	Omni	H8,I8	19.36	31.53 @ 49.39 dB
	DPP	H8,I8	23.56	43.3 @ 43.9 dB
Dir 7,8,1,2	Omni	G8,H8,I8,J8	26.07	64.58 @ 53 dB
	Omni	H8,I8	18.64	39 @ 53.38 dB
	DPP	H8,I8	20.91	49.13 @ 47.3 dB

Examination of MIMO gain in isolation

The capacity due to multipath decorrelation of the channel alone was examined with a fixed SNR value, arbitrarily assigned at 30 dB (refer to the *SNR = 30 dB* column of Table 3). For either receive array configuration, a 4 x 4 MIMO system employing an omnidirectional transmit array outperforms a $4 \times 2_2$ system having two dual polarised patch antennas. Section 4.4.1 discussed how omnidirectional discone receive elements develop greater MIMO capacity under fixed SNR conditions than

directional dipole counterparts by being more sensitive to multipath. Similarly, omnidirectional transmit elements are able to excite greater multipath in a rich scattering environment than a dual polarised patch, allowing greater capacity.

With available subchannels doubled, two dual-polarised patch elements may be expected to show grater capacity than two omnidirectional, single polarisation antennas. Considering alternate receive elements (Figure 30, left), the 4 x 2_2 system using a pair of dual polarised patches at the transmit array develops 4.2 bits/s/Hz capacity more than the 4 x 2 system with two omnidirectional transmit antennas.

As expected based on observations in section 4.4.1 above, receive array combinations directed towards the transmitter lowers capacity for all transmit antenna combinations examined under fixed SNR conditions. Receive array configuration choices maximising channel decorrelation by minimising direct paths and the use of omnidirectional transmit antennas exhibits optimal capacity under conditions of equal power reception.

Examination of MIMO gain and channel gain combined

Corroborating earlier discussions (section 4.4.1) regarding high SNR addressing inherent capacity deficits in correlated MIMO channels, adjacent receive elements directed at the transmit array show greatest capacity when actual SNR is considered.

While issues such as array packaging may suggest the use of dual-polarised patch elements in specific circumstances, omnidirectional antenna arrays would be a better choice for maximising capacity in most situations. Table 3 shows that even the suboptimal case of MIMO systems using alternate receive elements with omnidirectional transmit elements outperforms the best-case dual polarised patch transmitter system.

4.4.3 Channel correlation

Channel correlation is a consequence of wireless communication employing multiple element arrays in a multipath environment. Mutual coupling between array elements and fading correlation (determined by the spatial distribution of scatters within the propagation medium) are commonly observed correlative mechanisms.

Mutual coupling is present in fixed arrays such as at the receiver, but absent in the synthetic arrays such as the transmitter presented in this thesis.

Consider a 4 x 4 MIMO system using four-element omnidirectional receive array in conjunction with a synthetic, variable length four-element omnidirectional transmit array. The receive array elements are arranged in a square pattern, with $q\lambda$: q = 1,4 adjacent element separation. The locations of the receiver and NLOS transmitter are shown in Figure 31.

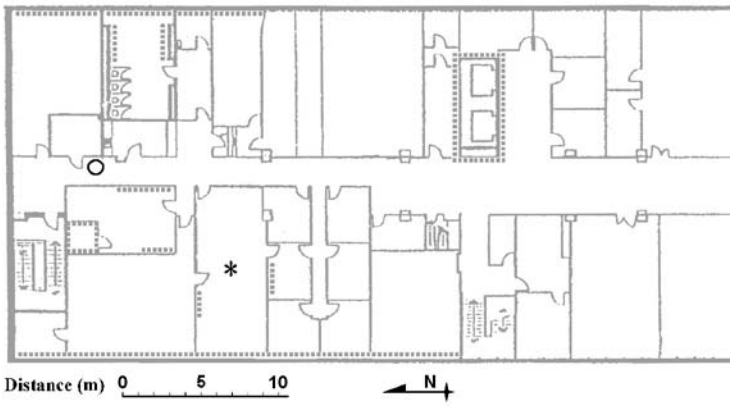

LEGEND

∗ *Omnidirectional* receive array.

O *Omnidirectional* transmit array.

Figure 31: NLOS omnidirectional transmit array and omnidirectional receive array used for correlation analysis

Linear arrays of four transmit antennas were selected from 17 possible element locations, arranged along the north-south axis, parallel to the hallway shown in Figure 31. Capacity of six MIMO systems with transmit array inter-element displacement varying from $n = 0d$ to $5d$ where

$$d = \frac{\lambda}{4}$$

is presented in Figure 32. Displayed capacity was calculated with a channel response matrix normalised as per section 2.7 with a fixed SNR of 30 dB.

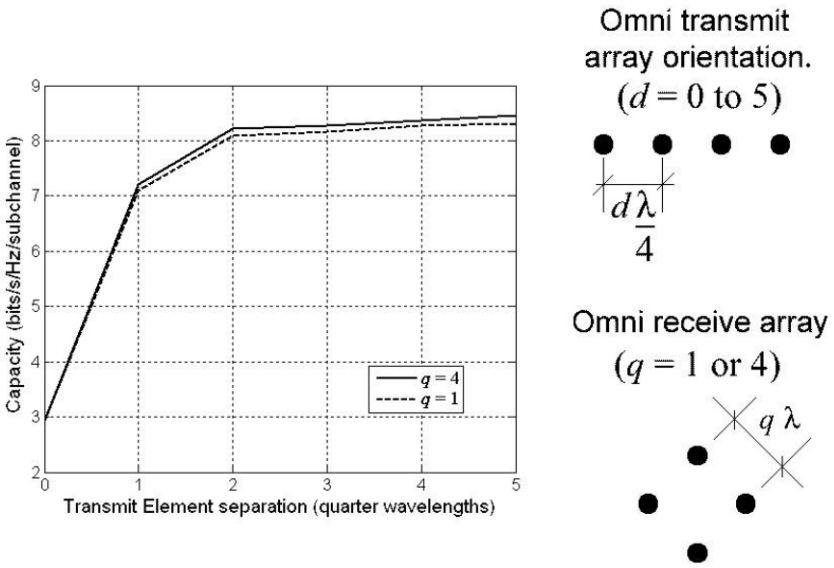

Figure 32: MIMO Capacity as a function of transmit array element displacement, for 1λ and 4λ separation at the receive array.

Despite the large physical dimensions of the omnidirectional array elements with respect to the operational wavelength, receive element displacement of 1λ appears sufficient to avoid mutual coupling in the circular receive array, with only small improvement observed with an increase to 4λ. Figure 32 suggests that λ/2 is the smallest practical separation between linear transmit array elements before fading correlation begins to significantly diminish MIMO capacity.

4.5 Singular value comparison of a range of indoor MIMO channels

Consider the hallway transmitter locations discussed in section 4.4.1 and shown in Figure 24. A comparative plot tracking the variation in singular values, averaged across frequency, of 4x4 MIMO systems using directional or omnidirectional receive arrays in conjunction with omnidirectional transmit arrays appears in Figure 33.

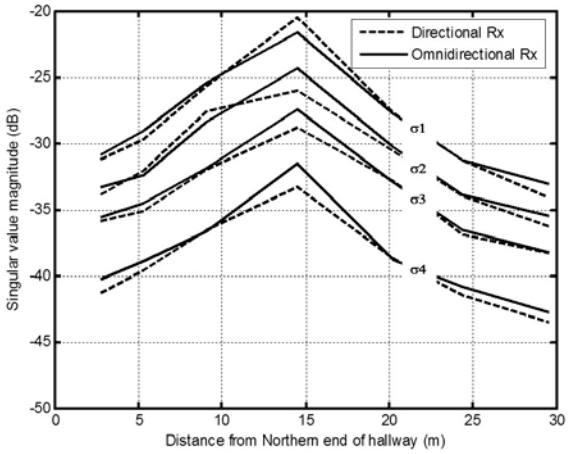

Figure 33: Comparative singular value behaviour of 4 x 4 MIMO systems along hallway.

The horizontal axis represents transmit array movement in a Southerly direction from Northern end along the central hallway of Figure 24. The highest directional singular values were found with one of eight possible groups of four adjacent elements. The transmit array for the MIMO system under discussion has four elements, linearly distributed 122.45 mm apart. Array alignment is perpendicular to the hall for the first and last location, but parallel for all others.

The most notable feature evident in Figure 33 is the singular value behaviour about the 14.5 m location. For the first three transmit array locations (2.8 m, 5.3 m and 9.1 m from the Northern hallway end), the omnidirectional array generally produces singular values of greater magnitude than the directional array. The situation changes as the transmitter moves closer the receive array. The variation in singular value distribution is most pronounced with the shortest separation between transmitter and receiver, occurring at approximately 14.5 m from the northern end. The horizontal axis of Figure 33 describes a procession from NLOS, through OLOS and back to NLOS. While not an example of true LOS, the OLOS environment present with the transmitter near 14m still demonstrates a comparative lack of multipath and a dominant signal. (see the *Rx3* subplot of the *DIRECTIONAL ARRAY* in Figure 22). The transition to OLOS tends to increase correlation in the channel response matrix, concentrating energy in the first singular value at the expense of the others. The reduced sensitivity of the directional array to multipath compared to the

omnidirectional array renders it more susceptible to increased channel matrix correlation.

4.6 Keyhole effect

As discussed in section 2.5, the keyhole effect manifests as an uncorrelated matrix, but with low rank. The measurement database was examined extensively over programs A, B and C for evidence of the keyhole effect. Irrespective of array element choice, arrangement or location, no channel response matrices, with varying degrees of correlation, were found to have less than full rank. The difficulty in observing the keyhole effect in actual measurements at cellular frequencies is in agreement with the conclusions of Almers *et al* in [18].

SUMMARY

Chapter 4 has presented frequency response, MIMO capacity and singular value analyses of some of the dataset gathered for this project and reviewed the operation of the **MATLAB** analysis software. It has been determined that for the indoor environment sampled, simple MIMO channels employing equal transmit power develop greatest capacity with omnidirectional arrays. Concluding remarks on this work are to follow in Chapter 5

Chapter 5

CONCLUSION

The limitations of traditional SISO communication techniques have been contrasted with MIMO, an alternative method to improve channel capacity in rich scattering environments. A literature review of the state of the art at the time of hardware development is presented. The operation of communication systems using MIMO architectures is discussed, with benefits and limitations to the use of multiple antenna arrays examined. Singular value decomposition and the theoretical maximum MIMO capacity limit are presented as analysis tools for MIMO channels.

The MIMO measurement hardware to characterise typical indoor office propagation environments is extensively covered. The development and implementation of the measurement system is presented, as is pertinent antenna theory and development, software operation and measurement protocols. This system was intended for quick deployment, to cost-effectively generate information about the propagation channel behaviour and to provide insight into the physical constraints and requirements of MIMO measurement programs in general. The equipment was wholly developed by the author, including the design and construction of a precision X-Y table capable of a repeatable positioning accuracy of 0.1 mm, suitable for a propagation measurement accuracy as low as -35 dB. The electronics was also

designed to bolster precision through the careful design of signal levels, the use of averaging in the network analyser and the calibration of the cables amplifiers and switches. As such, measurements taken with the hardware described in this thesis would be suitable for channel models requiring SNR to be as good as 29 dB (for a 6 dB margin). The equipment comfortably exceeds the requirements needed for today's wireless local area network (WLAN) standards. For example, the IEEE802.11a standard uses modulations up to 64QAM and specifies a transmission accuracy (or error vector magnitude) of –25 dB. This would call for a channel accuracy of greater than –25 dB – 6 dB margin = -31 dB to not dominate the performance of the link. The measurement equipment clearly exceeds these requirements.

For each of the three measurement campaigns undertaken, analyses of frequency and time domain responses, singular value decomposition and capacity of measured MIMO data are presented. A review of the **MATLAB** analysis software specifically written to examine the data in detail is provided.

The use of directional dipole receive arrays and dual polarised patch transmit arrays are compared in terms of MIMO capacity and singular values to the use of omnidirectional elements. For the indoor environment sampled, simple MIMO channels employing equal transmit power develop greatest capacity with omnidirectional arrays; the two examples of directional array elements used showed lower capacity than that achieved with omni-directional arrays. Creating a 4 x 4 system from both polarisations of two dual-polarised transmit elements only generated 60.4% of the capacity of four separate omni-directional antennas. However, the doubling of available sub channels afforded with the use of dual-polarised patch elements was shown to improve on omnidirectional capacity by as much as 26% for the same number of antennas.

SNR at the receiver has been shown to be a significant determinant of MIMO capacity, even in the presence of channel correlation. Fading correlation begins to have an impact on MIMO capacity as omnidirectional transmit array element displacement falls below $\lambda/2$. Mutual coupling between omnidirectional receive elements was not observed even at the smallest separation of λ.

The keyhole effect was not observed anywhere in the indoor propagation environment considered, consistent with [18].

Further work

Some of the possibilities for further work with this project would be to examine the following:

- Array spatial correlation with resolution better than $\lambda/4$.
- Mutual coupling at the receive array.
- Dual polarised patch measurements at different locations, including pointing away from the receive array and with an omnidirectional receive array.
- Hardware optimisation
    - -Reduce measurement time.
    - -Increase measurement flexibility with rotating head and z axis at transmitter to give more degrees of freedom (particularly useful for characterising handheld antennas in MIMO operation).
    - -Replacing the cumbersome double shielded transmit cable with a swept oscillator at transmit table with an optical link to network analyser reference clock.

PUBLICATIONS

CONFERENCE PAPERS

- Mewburn, M., Faulkner, M., Tan, Y. *A Comparison of Base Station Antenna Arrays in Multiple-Input Multiple-Output Wireless Systems*. in *Proc. 4th ATcrc Telecommunications and Networking Conference and Workshop*. 2004. Perth, Australia.
- Tan, Y., Pereira, M., Mewburn, M., Faulkner, M. *Investigation of Singular Value Distributions of MIMO Channels in Indoor Environment.* in *Proc. 2nd ATcrc Telecommunications and Networking Conference and Workshop*. 2002. Fremantle, WA Australia.

PAPERS SUPPORTING A POSTER PRESENTATION

- Mewburn, M. *Indoor MIMO channel characterisation.* in *Proc. 2nd ATcrc Telecommunications and Networking Conference and Workshop*. 2002. Fremantle, WA, Australia.

REFERENCES

1. Shannon, C.E., *A Mathematical Theory of Communication.* Bell System Technical Journal, 1948. **27**: p. 379-423, 623-656.
2. Foschini, G.J. and M.J. Gans, *On limits of wireless communications in a fading environment when using multiple antennas.* Wireless Personal Communications, 1998. **6**(3): p. 315-335.
3. Jungnickel, V., V. Pohl, and C. von Helmolt. *Experiments on the element spacing in multi-antenna systems*. in *Vehicular Technology Conference, 2003. VTC 2003-Spring. The 57th IEEE Semiannual.* 2003.
4. Bliss, D.W., et al. *MIMO environmental capacity sensitivity*. in *Signals, Systems and Computers, 2000. Conference Record of the Thirty-Fourth Asilomar Conference on*. 2000.
5. Winters, J.H., *On the capacity of radio communications systems with diversity in Rayleigh fading environments.* IEEE J. Sel. Areas Commun., 1987. **vol. 5, no. 5**: p. 871–878.
6. Telatar, I.E., *Capacity of multi-antenna Gaussian channels.* Eur. Trans. Telecommunication, 1999. **vol. 10, no. 6**: p. 585–595.
7. McNamara, D.P., et al., *Capacity variation of indoor multiple-input multiple-output channels.* Electronics Letters, 2000. **36**(24): p. 2037-2038.
8. Wallace, J.W., Jensen, M. A., Swindlehurst, A. L. and Jeffs, B. D., *Experimental Characterization of the MIMO Wireless Channel: Data Acquisition and Analysis*. IEEE Trans. Wireless Commun., 2003. **Vol. 2**: p. 335–343.
9. Chizhik, D., et al. *Multiple input multiple output measurements and modeling in Manhattan.* in *Vehicular Technology Conference, 2002. Proceedings. VTC 2002-Fall. 2002 IEEE 56th*. 2002.

10. Martin, C.C., J.H. Winters, and N.R. Sollenberger. *Multiple-input multiple-output (MIMO) radio channel measurements*. in *Vehicular Technology Conference, 52nd IEEE VTS-Fall.* 2000.
11. Yu, K., et al. *Second order statistics of NLOS indoor MIMO channels based on 5.2 GHz measurements*. in *Global Telecommunications Conference, 2001. GLOBECOM '01. IEEE*. 2001. San Antonio, Tx.
12. McNamara, D.P., M.A. Beach, and P.N. Fletcher. *Experimental investigation of the temporal variation of MIMO channels*. in *Vehicular Technology Conference, 2001. VTC 2001 Fall. IEEE VTS 54th*. 2001.
13. Molisch, A.F., et al., *Capacity of MIMO systems based on measured wireless channels.* Selected Areas in Communications, IEEE Journal on, 2002. **20**(3): p. 561-569.
14. Molisch, A.F., et al. *Measurement of the capacity of MIMO systems in frequency-selective channels*. in *Proc. IEEE 53rd Veh. Technol. Conf.* 2001.
15. Steinbauer, M., A.F. Molisch, and E. Bonek, *The double-directional radio channel.* Antennas and Propagation Magazine, IEEE, 2001. **43**(4): p. 51-63.
16. Jiang, J.-S. and M.A. Ingram. *Enhancing measured MIMO capacity by adapting the locations of the antenna elements*. in *Personal, Indoor and Mobile Radio Communications, 2002. The 13th IEEE International Symposium on*. 2002.
17. Jiang, J., M.F. Demirkol, and M.A. Ingram. *Measured Capacities at 5.8 GHz of Indoor MIMO Systems with MIMO Interference*. in *IEEE Vehicular Technology Conference,*. 2003.
18. Almers, P., F. Tufvesson, and A.F. Molisch, *Measurement of keyhole effect in a wireless multiple-input multiple-output (MIMO) channel.* Communications Letters, IEEE, 2003. **7**(8): p. 373-375.
19. Jiang, J. and M.A. Ingram. *Path Models and MIMO Capacity for Measured Indoor Channels at 5.8 GHz*. in *9th International Symposium on Antenna Technology and Applied Electromagnetics*. 2002.
20. Almers, P., et al. *The effect of horizontal array orientation on MIMO channel capacity*. in *Vehicular Technology Conference, 2003. VTC 2003-Spring. The 57th IEEE Semiannual*. 2003.
21. Siew, J., et al., *A Channel Estimation Method for MIMO-OFDM Systems.* London Communications Symposium, 2002.

22. Ivrlac, M., T. and Nossek, J., A., *Correlated fading in MIMO systems - blessing or curse?* 39th Annual Allerton Conference on Communication, Control and Computing, 2001.
23. McNamara, D.P., et al. *Initial investigation of multiple-input multiple-output (MIMO) channels in indoor environments*. in *Communications and Vehicular Technology, 2000. SCVT-200. Symposium on*. 2000.
24. Wallace, J.W. and M.A. Jensen. *Measured characteristics of the MIMO wireless channel*. in *Vehicular Technology Conference, 2001. VTC 2001 Fall. IEEE VTS 54th*. 2001.
25. Kyritsi, P. and D. Chizhik, *Capacity of multiple antenna systems in free space and above perfect ground.* Communications Letters, IEEE, 2002. **6**(8): p. 325-327.
26. Svantesson, T. *An antenna solution for MIMO channels: the multimode antenna*. in *Signals, Systems and Computers, 2000. Conference Record of the Thirty-Fourth Asilomar Conference on*. 2000.
27. Wennstrom, M. and T. Svantesson. *An antenna solution for MIMO channels: the switched parasitic antenna*. in *Personal, Indoor and Mobile Radio Communications, 2001 12th IEEE International Symposium on*. 2001.
28. Karamalis, P.D., N.D. Skentos, and A.G. Kanatas, *Adaptive Antenna Subarray Formation for MIMO Systems*. Wireless Communications, IEEE Transactions on, 2006. **5**(11): p. 2977-2982.
29. Rappaport, T.S., *Wireless Communications: Principle and Practice*. 2002, NJ, 07458: Prentice Hall PTR. 203-204.
30. Neirynck, D., et al. *Channel Characterisation for Personal Area Networks*. in *EURO-COST*. 2005. Lisbon, Portugal.
31. Tang, Z. and A.S. Mohan, *Experimental investigation of indoor MIMO Ricean channel capacity*. Antennas and Wireless Propagation Letters, 2005. **4**: p. 55-58.
32. Tan, Y., Pereira, M., Mewburn, M., Faulkner, M. *Investigation of Singular Value Distributions of MIMO Channels in Indoor Environment*. in *Proc. 2nd ATcrc Telecommunications and Networking Conference and Workshop*. 2002. Fremantle, Australia.

33. Khalighi, M.A., et al. *Water filling capacity of Rayleigh MIMO channels*. in *Proc. IEEE 12th Int. Symp. on Personal, Indoor and Mobile Radio Comm.* 2001. San Diego, CA.
34. *MC78XX/LM78XX/MC78XXA 3-Terminal 1A Positive Voltage Regulator.* Fairchild Semiconductor Datasheet, (Figure 10).
35. Tan, Y. and M. Faulkner. *Effect of the leakage between elements on the measured capacity of indoor multiple-input multiple-output channels*. in *Personal, Indoor and Mobile Radio Communications, 2002. The 13th IEEE International Symposium*. 2002.
36. *BROADBAND MONOLITHIC AMPLIFIERS, DC to 8 GHz.* Mini-Circuits datasheet, "Typical biasing configuration".
37. Row, J.S., Yeh, S. H., Wong, K. L., *Compact Dual-Polarized Microstrip Antennas.* Microwave and Optical Technology Letters, 2000. **27**: p. 284-287.
38. Browne, D.W., M.W. Browne, and M.P. Fitz, *Singular Value Decomposition of Correlated MIMO Channels.* IEEE GLOBECOM, Conf. Proc., 2006: p. 1 - 6.

APPENDIX A

SCHEMATICS

Schematic 1: Dual stepper motor controller

Schematic 2: RF switch

Schematic 3: RF switch controller

Schematic 4: Low noise amplifier

Schematic 1: Dual stepper motor controller

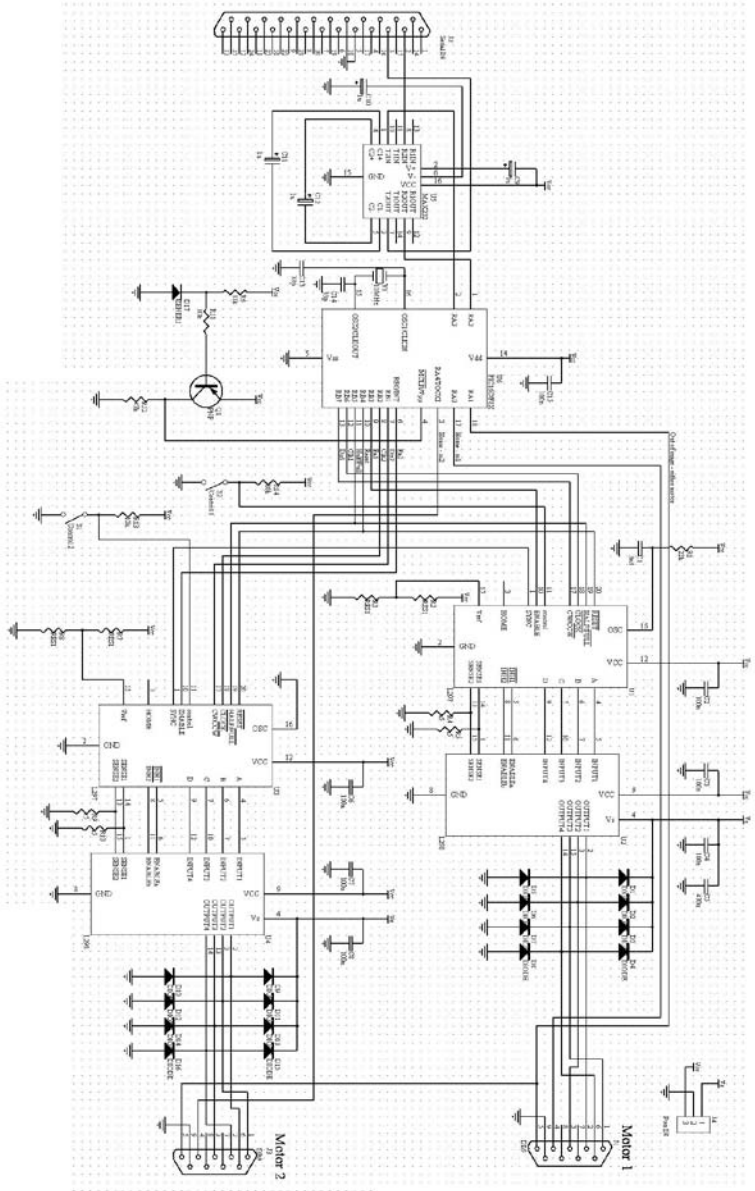

Schematic 2: RF switch

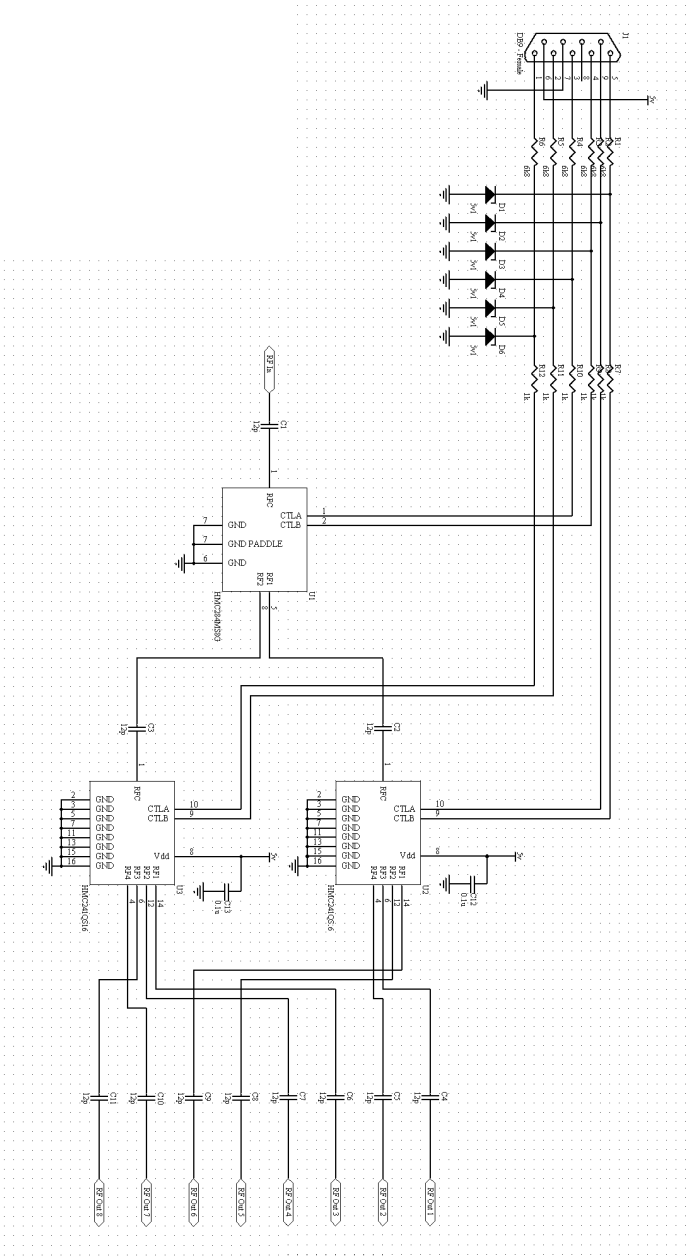

Schematic 3: RF switch controller

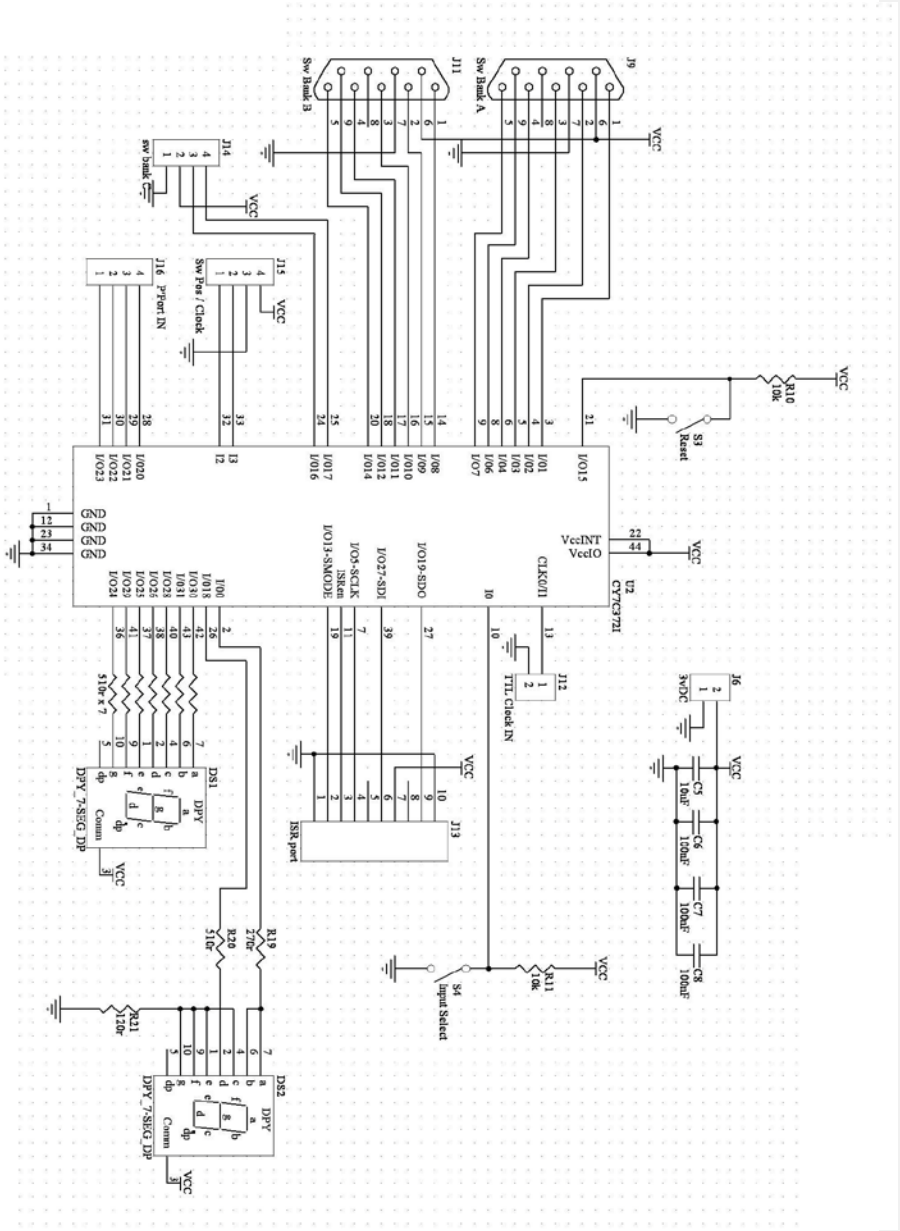

Schematic 4: Low noise amplifier

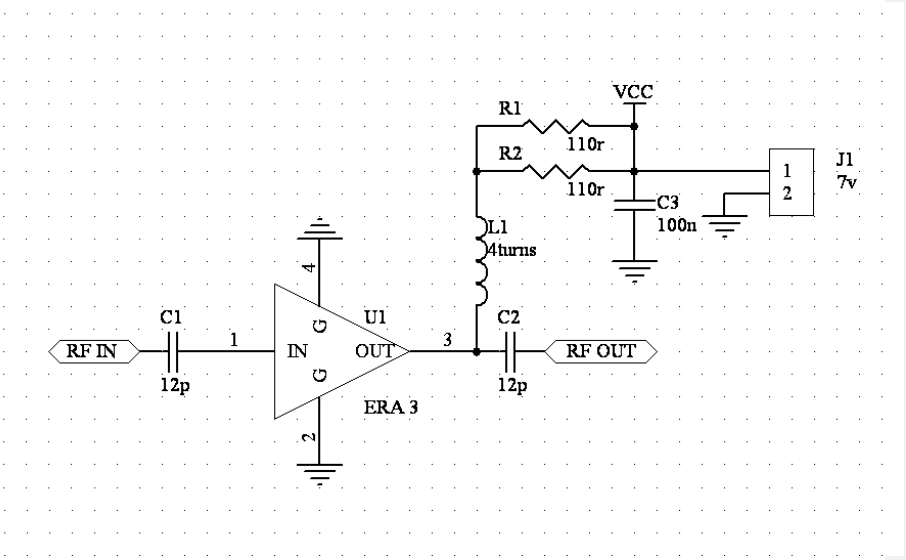

APPENDIX B

FIRMWARE

VHDL code for controller CPLD.

```
library ieee;
use ieee.std_logic_1164.all;

entity control_box is port(
  clk:in std_logic;
  clk_pport:in std_logic;
  reset:in std_logic;
  pos_per_clkA:in std_logic;
  pos_per_clkB:in std_logic;
  parallel_port: in std_logic_vector(3 downto 0);
  bankA:out std_logic;
  bankB:out std_logic;
  clinesA:out std_logic_vector(5 downto 0);
  clinesB:out std_logic_vector(5 downto 0);
  clinesC:out std_logic_vector(1 downto 0);
  dlines:out std_logic_vector(6 downto 0)
);
end control_box;

architecture control_box of control_box is

-- state assignments

--type StateType is
(switch1,switch2,switch3,switch4,switch5,switch6,switch7,switch8,switch9,switch10,switch11,switch12,
switch13,switch14,switch15,switch16);
constant switch1:std_logic_vector(3 downto 0)        :="0000";
constant switch2:std_logic_vector(3 downto 0)        :="0001";
constant switch3:std_logic_vector(3 downto 0)        :="0010";
constant switch4:std_logic_vector(3 downto 0)        :="0011";
constant switch5:std_logic_vector(3 downto 0)        :="0100";
```

```
constant switch6:std_logic_vector(3 downto 0)          :="0101";
constant switch7:std_logic_vector(3 downto 0)          :="0110";
constant switch8:std_logic_vector(3 downto 0)          :="0111";
constant switch9:std_logic_vector(3 downto 0)          :="1000";
constant switch10:std_logic_vector(3 downto 0)         :="1001";
constant switch11:std_logic_vector(3 downto 0)         :="1010";
constant switch12:std_logic_vector(3 downto 0)         :="1011";
constant switch13:std_logic_vector(3 downto 0)         :="1100";
constant switch14:std_logic_vector(3 downto 0)         :="1101";
constant switch15:std_logic_vector(3 downto 0)         :="1110";
constant switch16:std_logic_vector(3 downto 0)         :="1111";

signal current_state,next_state:std_logic_vector(3 downto 0);

--signal current_state,next_state:StateType;
signal clinesA1,clinesA2,clinesB1,clinesB2:std_logic_vector(5 downto 0);
signal dlines1,dlines2:std_logic_vector(6 downto 0);



begin

    state_comb:process(current_state,clk_pport,pa
    rallel_port,pos_per_clkA,pos_per_clkB)

     begin
      case current_state is
        when switch1 =>
          clinesA1 <= "001001";
          clinesB1 <= "001001";
          dlines1  <= "1111001";
          next_state<=switch2;
        when switch2 =>
          clinesA1 <= "001101";
          clinesB1 <= "001001";
          dlines1  <= "0100100";
          next_state<=switch3;
        when switch3 =>
          clinesA1 <= "000010";
          clinesB1 <= "001001";
          dlines1  <= "0110000";
          next_state<=switch4;
        when switch4 =>
          clinesA1 <= "010010";
          clinesB1 <= "001001";
          dlines1  <= "0011001";
          if pos_per_clkA ='0' and pos_per_clkB ='1'
then
            next_state <= switch1;
          else
            next_state <= switch5;
          end if;
        when switch5 =>
          clinesA1 <= "000101";
          clinesB1 <= "001001";
          dlines1  <= "0010010";
          next_state<=switch6;
        when switch6 =>
          clinesA1 <= "000001";
          clinesB1 <= "001001";
          dlines1  <= "0000010";
          next_state<=switch7;
        when switch7 =>
          clinesA1 <= "110010";
          clinesB1 <= "001001";
          dlines1  <= "1111000";
```

```
      next_state<=switch8;
    when switch8 =>
      clinesA1 <= "100010";
      clinesB1 <= "001001";
      dlines1  <= "0000000";
      if pos_per_clkA ='1' and pos_per_clkB ='0'
then
        next_state <= switch9;
      else
       next_state <= switch1;
      end if;
    when switch9 =>
      clinesB1 <= "001001";
      clinesA1 <= "001001";
      dlines1  <= "1111001";
      next_state<=switch10;
    when switch10 =>
      clinesB1 <= "001101";
      clinesA1 <= "001001";
      dlines1  <= "0100100";
      next_state<=switch11;
    when switch11 =>
      clinesB1 <= "000010";
      clinesA1 <= "001001";
      dlines1  <= "0110000";
      next_state<=switch12;
    when switch12 =>
      clinesB1 <= "010010";
      clinesA1 <= "001001";
      dlines1  <= "0011001";
      next_state<=switch13;
    when switch13 =>
      clinesB1 <= "000101";
      clinesA1 <= "001001";
      dlines1  <= "0010010";
      next_state<=switch14;
    when switch14 =>
      clinesB1 <= "000001";
      clinesA1 <= "001001";
      dlines1  <= "0000010";
      next_state<=switch15;
    when switch15 =>
      clinesB1 <= "110010";
      clinesA1 <= "001001";
      dlines1  <= "1111000";
      next_state<=switch16;
    when switch16 =>
      clinesB1 <= "100010";
      clinesA1 <= "001001";
      dlines1  <= "0000000";
      next_state <= switch1;
    when others =>
      dlines1  <= "1001001";
      clinesB1 <= "001001";
      clinesA1 <= "001001";
      end case;
  end process;

switch_decoder:process(parallel_port)
 begin
    case parallel_port is
    when "0000" =>          -- switch 1
      clinesA2 <= "001001";
      clinesB2 <= "001001";
      dlines2  <= "1111001";
    when "0001" =>          -- switch 2
      clinesA2 <= "001101";
      clinesB2 <= "001001";
      dlines2  <= "0100100";
    when "0010" =>          -- switch 3
      clinesA2 <= "000010";
      clinesB2 <= "001001";
      dlines2  <= "0110000";
    when "0011" =>          -- switch 4
      clinesA2 <= "010010";
      clinesB2 <= "001001";
      dlines2  <= "0011001";
    when "0100" =>          -- switch 5
      clinesA2 <= "000101";
      clinesB2 <= "001001";
      dlines2  <= "0010010";
    when "0101" =>          -- switch 6
      clinesA2 <= "000001";
      clinesB2 <= "001001";
      dlines2  <= "0000010";
    when "0110" =>          -- switch 7
      clinesA2 <= "110010";
      clinesB2 <= "001001";
      dlines2  <= "1111000";
    when "0111" =>          -- switch 8
```

```
    clinesA2 <= "100010";
    clinesB2 <= "001001";
    dlines2  <= "0000000";
  when "1000" =>              -- switch 9
    clinesB2 <= "001001";
    clinesA2 <= "001001";
    dlines2  <= "1111001";
  when "1001" =>              -- switch 10
    clinesB2 <= "001101";
    clinesA2 <= "001001";
    dlines2  <= "0100100";
  when "1010" =>              -- switch 11
    clinesB2 <= "000010";
    clinesA2 <= "001001";
    dlines2  <= "0110000";
  when "1011" =>              -- switch 12
    clinesB2 <= "010010";
    clinesA2 <= "001001";
    dlines2  <= "0011001";
  when "1100" =>              -- switch 13
    clinesB2 <= "000101";
    clinesA2 <= "001001";
    dlines2  <= "0010010";
  when "1101" =>              -- switch 14
    clinesB2 <= "000001";
    clinesA2 <= "001001";
    dlines2  <= "0000010";
  when "1110" =>              -- switch 15
    clinesB2 <= "110010";
    clinesA2 <= "001001";
    dlines2  <= "1111000";
  when "1111" =>              -- switch 16
    clinesB2 <= "100010";
    clinesA2 <= "001001";
    dlines2  <= "0000000";
 when others =>
   clinesB2 <= "001001";
   clinesA2 <= "001001";
   dlines2  <= "1001001";
end case;
end process;
```

```
mux:process(clk_pport,dlines1,dlines2,clinesA1
,clinesA2,clinesB1,clinesB2)
 begin
  if (clk_pport='1') then
    dlines  <= dlines1;
    clinesA <= clinesA1;
    clinesB <= clinesB1;
  else
    dlines  <= dlines2;
    clinesA <= clinesA2;
    clinesB <= clinesB2;
  end if;
 end process;

mux2:process(clk_pport,current_state,parallel_
port)
 begin
  if (clk_pport='1') then
    if (current_state(3) <= '0')  then
      bankA <= '0';
      bankB <= '1';
      clinesC <= "10";
    else
      bankA <= '1';
      bankB <= '0';
      clinesC <= "01";
  end if;
    else
      if (parallel_port(3) = '1') then
        bankA <= '1';
        bankB <= '0';
        clinesC <= "10";
      else
        bankA <= '0';
        bankB <= '1';
        clinesC <= "01";
      end if;
    end if;
 end process;

 state_clock:process(clk,reset)
 begin
  if (reset='0') then
```

```
        current_state <= switch1;
    elsif (clk'event and clk='0') then
        current_state <= next_state;
    end if;
  end process state_clock;
end architecture control_box;
```

CPLD pin assignments.

```
Attribute PIN_NUMBERS of clinesa(0) is "3" ;
Attribute PIN_NUMBERS of clinesa(1) is "4" ;
Attribute PIN_NUMBERS of clinesa(2) is "5" ;
Attribute PIN_NUMBERS of clinesa(3) is "6" ;
Attribute PIN_NUMBERS of clinesa(4) is "8" ;
Attribute PIN_NUMBERS of clinesa(5) is "9" ;

Attribute PIN_NUMBERS of clinesb(0) is "14" ;
Attribute PIN_NUMBERS of clinesb(1) is "15" ;
Attribute PIN_NUMBERS of clinesb(2) is "16" ;
Attribute PIN_NUMBERS of clinesb(3) is "17" ;
Attribute PIN_NUMBERS of clinesb(4) is "18" ;
Attribute PIN_NUMBERS of clinesb(5) is "20" ;

Attribute PIN_NUMBERS of clinesc(0) is "25" ;
Attribute PIN_NUMBERS of clinesc(1) is "24" ;

Attribute PIN_NUMBERS of pos_per_clka is "33" ;
Attribute PIN_NUMBERS of pos_per_clkb is "32" ;

Attribute PIN_NUMBERS of dlines(0) is "42" ;
Attribute PIN_NUMBERS of dlines(1) is "43" ;
Attribute PIN_NUMBERS of dlines(2) is "40" ;
Attribute PIN_NUMBERS of dlines(3) is "38" ;
Attribute PIN_NUMBERS of dlines(4) is "37" ;
Attribute PIN_NUMBERS of dlines(5) is "41" ;
Attribute PIN_NUMBERS of dlines(6) is "36" ;

Attribute PIN_NUMBERS of banka is "2" ;
Attribute PIN_NUMBERS of bankb is "26" ;

Attribute PIN_NUMBERS of clk is "13" ;
Attribute PIN_NUMBERS of reset is "21" ;
Attribute PIN_NUMBERS of clk_pport is "10" ;

Attribute PIN_NUMBERS of parallel_port(0) is "28" ;
Attribute PIN_NUMBERS of parallel_port(1) is "29" ;
Attribute PIN_NUMBERS of parallel_port(2) is "30" ;
Attribute PIN_NUMBERS of parallel_port(3) is "31" ;
```

APPENDIX C

DUAL POLARISED PATCH ANTENNA DIMENSIONS.

Parameter	***Dimension (mm)***
Ground plane	57 x 57
Patch	25 x 25
Slot width	1
Inside slot length	5.5
Slot separation	5
Feed point to edge	8.2

APPENDIX D

MIMO MEASUREMENT ANALYSIS FILES

Use of the MATLAB analysis software requires the following directory structure and *MIMO Analysis* contents for correct operation:

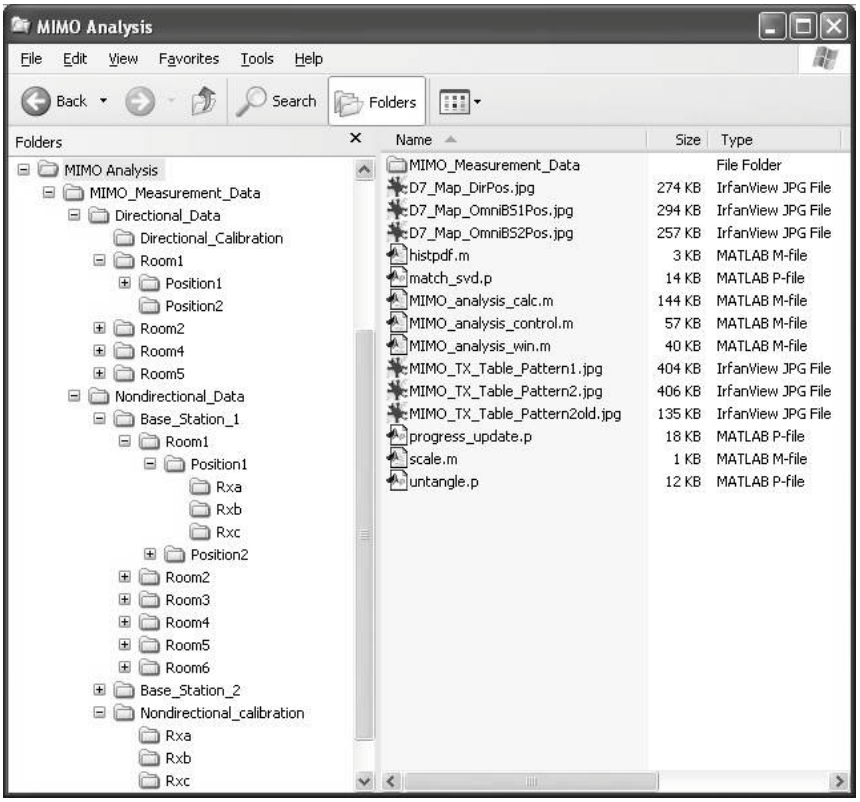

APPENDIX E

DIRECTIONAL ARRAY CAPACITY FOR GROUPS OF FOUR RECEIVE ELEMENTS MOVING SEQUENTIALLY AROUND THE ARRAY

Rx array	Transmitter position within Room 4						
elements	1	2	3	4	5	6	7
1 to 4	32.789	33.494	31.921	29.301	32.006	31.655	29.866
2 to 5	32.437	33.246	32.495	29.248	32.771	32.994	30.751
3 to 6	31.759	33.635	30.798	27.139	32.647	33.027	31.249
4 to 7	32.534	33.924	32.326	33.334	32.038	32.996	31.416
5 to 8	32.426	34.894	34.244	32.349	33.188	33.134	32.011
6 to 1	31.402	33.234	32.485	33.526	33.828	33.713	32.81
7 to 2	32.781	32.665	32.633	33.79	33.584	33.543	31.196
8 to 3	33.366	33.679	32.104	28.208	34.231	32.825	30.214